

Supporting Information

Effective Intermediate-Spin Iron in O₂-Transporting Heme Proteins

Nils Schuth¹, Stefan Mebs¹, Dennis Huwald², Pierre Wrzolek³, Matthias Schwalbe³,

Anja Hemschemeier², Michael Haumann^{1*}

¹Freie Universität Berlin, Department of Physics, 14195 Berlin, Germany

²Ruhr-Universität Bochum, Department of Plant Biochemistry, Photobiotechnology, 44801
Bochum, Germany

³Humboldt-Universität zu Berlin, Department of Chemistry, 12489 Berlin, Germany

Contents:

Experimental details

Computational details

Supporting discussion

Table S1: Fe K-edge and $K\beta_{1,3}$ line energies of heme species

Table S2: Interatomic distances in heme species from XAS and XRD

Table S3: Bond lengths/angles and Mulliken spin densities in porphyrins/hemes from DFT

Table S4: Natural orbitals in active space from CASSCF calculations

Table S5: Summary of CASSCF calculations with active spaces shown in Table S4

Table S6: Atomic orbital contributions to MOs from CASSCF for **oxy**

Figure S1: Time-resolved energy-sampling $K\beta$ XES

Figure S2: Optical absorption spectra of MB and HB

Figure S3: Lower-resolution XANES and EXAFS spectra of MB and HB at 20 K and 260 K

Figure S4: Interatomic distances from EXAFS analysis

Figure S5: Higher-resolution XANES spectra of MB and HB

Figure S6: Temperature-independence of $K\beta$ line ratios in MB and HB

Figure S7: Structures and $K\beta$ spectra of non-porphyrin compounds

Figure S8: Purity of $K\beta$ spectra of oxy MB/HB

Figure S9: Fit analysis of $K\beta$ main-line spectra

Figure S10: Fit results of $K\beta$ spectra

Figure S11: Correlations from $K\beta$ fit analysis

Figure S12: X-ray induced species modifications

Figure S13: Pre-edge absorption (ctv) and $K\beta$ satellite emission (vte) spectra of MB/HB

Figure S14: Structures and XAS/XES data for porphyrin compounds

Figure S15: $K\beta'$ -detected ctv spectra of MB/HB

Figure S16: Spin densities and target/source MOs for ctv/vte transitions in porphyrins

Figure S17: Heme ctv/vte spectra for structure variation from (TD)DFT

Figure S18: Calculated ctv/vte spectra of heme species and target/source MOs

Figure S19: DFT energies and electron densities for **oxy** for Fe-O₂ bond geometry variation

Figure S20: CASSCF data for active space and Fe-O₂ geometry variation

Chart S1: Coordinates of geometry-optimized heme and porphyrin structures.

Chart S2: Example of input files for (TD)DFT and MP2/CASSCF

Supporting References

Experimental details

X-ray spectroscopy. High-resolution Fe K-edge XANES/K β -XES spectra were collected at the triple-undulator beamline ID26 at ESRF (Grenoble, France) using our previously established methods (samples held in a liquid-helium cryostat from Cryovac, excitation energy varying by a Si[311] double-crystal monochromator with ~ 0.2 eV bandwidth, providing a flux of $\sim 10^{12}$ photons per second and mm^2 at the Fe K-edge) (1-5). The X-ray beam was focused by mirrors to give a flat profile at about (vertical) ~ 0.2 - 0.3 mm and (horizontal) ~ 0.3 - 0.4 mm. A sharp spot size on the sample was defined by slits. Rapid-scan (~ 1 s) XANES spectra were obtained in transmission mode (porphyrin compound powder = microcrystalline samples) and by broad-band total (K α) fluorescence detection (scintillation detector with ~ 20 cm^2 area at 90° and ~ 1 m distance to the sample shielded by a 10 μM Mn foil against scattered incident X-rays) or narrow-band K β fluorescence detection (HB/MB) using the emission spectrometer. XES data were collected on a vertical-plane Rowland-circle spectrometer with an avalanche photodiode detector (emission energy bandwidth ~ 1 eV, 5 spherical Ge[620] crystal analyzers at $R = 1000$ mm, and shielded by a ~ 1 mm slit against scattered incident X-rays) (1). The X-ray beam was appropriately attenuated by stacked Al foils of each 20 μm thickness (filter box from XIA, ~ 30 % flux attenuation at the Fe K-edge per foil). X-ray exposure time periods for unperturbed data collection were determined from X-ray fluorescence timescans and successive XANES scans on single sample spots used to monitor X-ray induced sample modifications. K β emission spectra were collected using a point-by-point time-resolved energy-sampling approach (~ 1 s data acquisition per 0.35 eV step) as previously described (for details see ref. (2) and Fig. S1). Monochromator and emission spectrometer energy axes were calibrated with a precision of ± 0.1 eV using a Gaussian fit to the elastic scattering peak of the incident X-rays for monochromator energy calibration and according calibration of the emission spectrometer energy (2). Lower-resolution XANES/EXAFS spectra were collected at beamline KMC-3 at BESSY (Helmholtz-Center Berlin; Si[111] double-crystal monochromator with ~ 2 eV bandwidth, single-element silicon-drift fluorescence detector from Bruker, samples held in a LHe-cryostat from Oxford) (6). Signal-to-noise ratios were improved by averaging of spectra (rapid-scan XAS, ≤ 150 scans; K β XES, ≤ 10 point-by-point data sets) collected on separate non-overlapping sample spots. XAS/XES spectra were processed (background subtraction, normalization) as described earlier (1). K β' amplitudes were derived from data points within 7044 – 7046 eV. k^3 -weighted EXAFS spectra were simulated with in-house software and phase functions from FEFF9 ($S_0^2 = 0.85$) (7).

Computational details

(TD)DFT. (TD)DFT (and MP2/CASSCF) calculations were performed on the Soroban computer cluster of the Freie Universität Berlin. The ORCA and Gaussian09 program packages for geometry-optimization of heme structures and spectral calculations (B3LYP functional, def2-TZVP basis set, COSMO solvation model ($\epsilon = 80.44$) in ORCA). Starting geometries for porphyrin compounds **2** and **3** were derived from the crystal structure of compound **1** or from crystal structures of MB (PDB entries 1A6N, 1A6G, 1CQ2) and HB (PDB entries 2DN1-3). Porphyrin ring and histidine side chains were truncated and saturated with protons in the heme model structures. During geometry optimization of heme structures, the C-atoms of the porphyrin and the distal histidine were restraint at their crystallographic positions. From the resulting wave-function files, frontier MOs and Mulliken spin densities were derived. Representative coordinates of porphyrin compound and heme structures are shown in Chart S1, representative input files for (TD)DFT are shown in Chart S2.

MP2/CASSCF. Geometries of heme and porphyrin structures were optimized using DFT (B3LYP functional, def2-TZVP and def2-TZVP/JK basis-sets) using the ORCA program (version 3.0.3) (8, 9). The generated wavefunction was used as initial guess for a Møller-Plesset second-order perturbation theory (MP2) calculation with resolution-of-identity (RI) approximation and the natural orbitals from the unrelaxed density were used for further calculations. For complete-active-space self-consistent-field (CASSCF) calculations, the active space was constructed by visual inspection of the separately localized internal and external space using the MP2 natural orbitals, including orbitals which involved iron and the axial ligands (Table S4). The active space was increasingly expanded (for example for **oxy** heme from (8,7) to (14,11) (electrons,MOs) until no further significant changes in the effective unpaired electron density (EUED) were observed (Tables S5 and S6, Fig. S20). CASSCF calculations were done using the RI approximation for the 'trafo' step. Electron densities were analyzed using hard-shell-weighting, i.e. the MO was assumed to be completely localized on the atom with its largest contribution. Effective unpaired electron densities were calculated using the density function of Takatsuka et. al. (10). The respective restricted-open-shell Hartree-Fock (ROHF) wavefunctions provided the expected number of 4 or 5 unpaired electrons. i.e. singly occupied MOs, for HS Fe(II) in **deoxy** or HS Fe(III) in porphyrin compound **3**. Input files for MP2/CASSCF are shown in Chart S2.

Supporting discussion

Relation of $K\beta$ main-line emission and metal spin state. The $K\beta$ main-line emission results from dipole-allowed radiative $3p \rightarrow 1s$ electronic decay after previous resonant (i.e. into metal 3d levels) or non-resonant (into the continuum) core level (1s) electron excitation (Figs. 2 and 3). For non-resonant excitation the sequence of states is: initial state, $1s^2 3p^6 3d^n$; intermediate state, $1s^1 3p^6 3d^n$; final state, $1s^2 3p^5 3d^n$. The line is split into the $K\beta_{1,3}$ and $K\beta'$ features due to spin-polarization of the $K\beta_{1,3}$ and $K\beta'$ features ($3p \rightarrow 1s$ decay) in response to strong metal($p-d$) electron exchange coupling (11-13). The relative line intensity and shape changes in response to a change in the nominal number of unpaired metal d-spins can be rationalized in a multiplet framework and are largely due to modulations of the exchange integrals between the 3p hole and the 3d electrons in the final state (11, 13-17). An increase of the $K\beta'$ emission intensity with respect to the $K\beta_{1,3}$ emission (for non-resonant excitation) due to coupling between an increasing number of (nominal) unpaired metal-d spins and the 3p hole in the final state (14, 15, 18, 19) has been shown for various first-row transition metal compounds with increasing oxidation and/or spin state (1, 5, 20-26). However, the $K\beta$ main line splitting and relative intensity and energy of the $K\beta'$ feature is further influenced by the covalency of the metal-ligand bonding (i.e. delocalization of metal-d orbitals onto the ligands) (1, 16). The latter effect has been shown to decrease the relative intensity of the $K\beta'$ feature significantly for example in iron compounds showing sulfur instead of nitrogen ligands at Fe(III) or Fe(II) centers (1) and in compounds with increasing bonding covalency and similar Fe(III) centers (16). For increasing numbers of unpaired Fe(d) spins, the slope of the correlation to the $K\beta'$ intensity was found to be smaller for iron in 'ionic' vs. 'covalent' coordination environments (1), meaning the $K\beta$ emission probes the effective rather than the formal Fe(d) spin count. Clear relations between the $K\beta$ main line spectral features and the (formal) Fe(d) spin count (such as an increase in $K\beta'$ intensity) therefore are only expected within relatively homogeneous series of compounds. We show that for the studied heme species in HB and MB and for the three porphyrin compounds, the $K\beta'$ intensities (or relative line energies, Figs. S9-S11) are described by the same linear relation to the formal Fe(d) spin count, with a slope that is similar to the one for the various studied non-porphyrin complexes. Accordingly, the heme species and the porphyrin compounds show similar overall covalency of the iron-ligand bonding, as expected, which is also close to the 'non-covalent' limit of, e.g., iron oxides. We note that this correlation holds for LS or HS, ferrous or ferric iron species with 0-5 unpaired Fe(d) spins, i.e. the spin count

changes dominate the correlation rather than the redox state. For **oxy** heme, the non-resonant $K\beta$ emission features indicated an effective unpaired Fe(d) spin count of two, which, due to the diamagnetic behaviour ($M = 1$) cannot be explained by higher spin states of iron. This result is in agreement with our CASSCF calculations revealing spin densities close to unity in two MOs with mostly Fe($d_{xz,yz}$) characters, which sum up to an effective unpaired electron density (EUED) of ~ 2 on iron. These findings establish a clear relation between the spectroscopy and theory results, meaning that the $K\beta$ emission is a measure of the effective Fe(d) spin count for systems showing a more ‘standard’ d-level occupancy with apparently rather innocent ligands (**deoxy** and **carboxy** hemes, porphyrin compounds) and for the more sophisticated metal-ligand bonding situation in **oxy** heme with the less innocent O_2 ligand.

Resonant excitation of $K\beta$ emission. For resonant 1s electron excitation into the valence levels at incident energies in the pre-K-edge absorption region, creation of an additional unpaired Fe(d) spin or spin pairing in the final state can occur (initial state, $1s^2 3p^6 3d^n$; intermediate state, $1s^1 3p^6 3d^{n+1}$; final state, $1s^2 3p^5 3d^{n+1}$). The resulting $K\beta$ spectrum (Fig. 2) reflects a transect through the so-called resonant inelastic X-ray scattering (RIXS) plane (i.e. intensity plotted vs. emission and excitation energy) in the direction of constant excitation energy (21, 27) and its shape depends on the excitation energy due to probing of different unoccupied valence, i.e. Fe(d), levels. We chose an energy for resonant excitation (7113 eV) that caused excitation into Fe(d) dominated MOs for all studied heme and porphyrin species, as supported by the computational results. The observed relation between the $K\beta'$ intensities and the Fe(d) spin count for resonant excitation may be explained according to the following considerations. (a) For HS Fe(II) in **deoxy** and porphyrin **2** and HS Fe(III) in porphyrin **3**, 1s α -spin excitation was not possible (all d-levels singly or doubly occupied) and 1s β -spin excitation resulted in spin pairing and therefore in a decrease of the respective unpaired Fe(d) count by one unit (i.e. from 4 to 3 or 5 to 4) so that the 3p/3d coupling and the related $K\beta'$ intensity were diminished. (b) For LS Fe(II) in **carboxy** and porphyrin **1**, 1s α - or β -spin excitation was possible (unoccupied e_g d-levels available) and resulted in an increase of the respective unpaired Fe(d) count by one unit (from 0 to 1) so that the 3p/3d coupling and the related $K\beta'$ intensity were increased. (c) For the ‘intermediate spin’ iron in **oxy**, 1s α/β -spin excitation was possible (unoccupied Fe(d_{z^2/x^2-y^2}) dominated MOs, singly occupied Fe($d_{xz/yz}$) dominated MOs) and (formally) resulted either in creation of an additional unpaired Fe(d) spin or in spin pairing, increasing or diminishing the unpaired Fe(d) count (from 2 to 3 or from 2 to 1) by one unit, so that the 3p/3d coupling and the related $K\beta'$ intensity were either increased or diminished, which resulted in an apparently unchanged

effective Fe(d) count (of 2) for **oxy** when compared to non-resonant excitation. In case (a), a 3p hole with the same (α) spin flavour as the unpaired Fe(d) spins in the final state was not created, whereas in cases (b) and (c) 3p holes with the same α/β spin flavour as the unpaired Fe(d) spins in the final state were created, so that 3p/3d coupling was enhanced in the latter cases vs. the former case, which accounted for the decreasing $K\beta'$ intensity for increasing Fe(d) counts, as opposed to non-resonant excitation. These considerations yielded an approximately linear relation between the $K\beta'$ intensity and the unpaired Fe(d) count for resonant excitation, provided further evidence that the $K\beta$ emission is a sensitive measure of the spin state, and supported that the iron center in **oxy** is in a higher spin state compared to **carboxy**, excluding a canonical LS Fe(II) species as suggested in the Pauling model. We note that a fully quantitative evaluation of $K\beta$ data from resonant excitation would have to include analysis of the complete multiplet structure as accessible via RIXS data, i.e. DFT calculation of the RIXS plane, which at present is not available in the ORCA program (8).

Narrow-band $K\beta$ detection of ctv spectra. X-ray pre-edge absorption spectra (ctv) reflect resonant 1s electron excitation into unoccupied valence levels and were collected using either (i) broad-band $K\alpha$ ('total fluorescence') or (ii) narrow-band $K\beta$ detection (Figs. 4, S5, S13, S14, S15) (5, 26). While in case (i) all unoccupied levels in the valence shell multiplet are probed and respective ctv spectra are similar to transmission-detected spectra, in case (ii) a subset of the multiplet is probed and the ctv spectrum represents a transect through the RIXS plane at constant emission energy. For detection in the $K\beta'$ region of iron (7045 eV) the expected ctv spectra are explained using a similar rationale as for resonantly excited $K\beta$ emission spectra (see above), meaning that respective ctv intensities are expected to be small for the absence of surplus unpaired Fe(d) spins and of a 3p hole with the same spin flavour in the final state and to increase for increasing numbers of unoccupied valence levels as targets for resonant excitation and thereby enhanced 3p/3d coupling. This rationale is confirmed by the small ctv intensities of HS Fe(II) and Fe(III) species in **deoxy** and porphyrins **2** and **3** and by the similar ctv intensities as for broad-band fluorescence detection of LS Fe(II) species in **carboxy** and porphyrin **1**. For **oxy**, the $K\beta'$ detected ctv spectrum retained significantly intensity exceeding the one of **deoxy**, but this intensity was diminished relative to **carboxy** compared to broad-band fluorescence detection. These findings supported that a canonical LS Fe(II) as in **carboxy** was not realized and that the iron center showed a higher spin state in **oxy**. We note that low-energy ctv transitions, as visible in the broad- and narrow-band ctv spectra of **oxy**, were not expected in the Pauling model and explained by transitions into MOs with dominant Fe($d_{xz,yz}$) characters as revealed by the CASSCF calculations.

Table S1: Fe K-edge and K $\beta_{1,3}$ line energies of heme species.

	K-edge energy [eV] ^a		K $\beta_{1,3}$ energy [eV] ^b	
	MB	HB	MB	HB
deoxy	7120.9(1)	7121.0(1)	7058.6(1)	7058.6(1)
carboxy	7122.3(1)	7122.2(1)	7057.9(1)	7058.0(1)
	[7122.4(4)]	[7122.3(3)]		[7057.9(2)]
oxy	7123.9(1)	7123.8(1)	7058.3(1)	7058.4(1)
	[7123.9(4)]	[7123.9(6)]		[7058.3(2)]

^aK-edge energies (at 50 % level) refer to mean lower-/higher-resolution XANES data in Figs. S3A and S5 or (in brackets) were estimated from spectra reported in literature (28-33), which were shifted so that respective energies for **deoxy** aligned with our data (the range of energy variations is given in parenthesis). ^bK $\beta_{1,3}$ line energies were determined from calculation of the 1st-moment (M) of spectra, $M = \Sigma [I(E)*E] / \Sigma [I(E)]$ in Fig. 2 within 7055-7062 eV (mean of 20/260 K data, energy range in parenthesis) or estimated from K β data in ref. (34) (in brackets, energies were shifted to match our **deoxy** value and energy differences scaled to match our data, estimated error in parenthesis).

Table S2: Interatomic distances in heme species from XAS and XRD.^a

	interatomic distance [Å]									
	Fe-C/O(=O)		Fe(-C/O)=O		Fe-N _{porphyrin}		Fe-N _{His}		Fe-C _{porphyrin/His}	
	XAS	XRD	XAS	XRD	XAS	XRD	XAS	XRD	XAS	XRD
MB										
deoxy	-	-	-	-	2.06(2)	2.04(2)	2.18(2)	2.20(2)	3.20	3.19
carboxy	1.79(1)	1.82(2)	2.97(3)	2.94(4)	2.00(1)	2.01(3)	2.09(2)	2.07(1)	3.18	3.15
oxy	1.91(2)	1.83(2)	3.03(2)	2.64(10)	2.04(1)	1.99(3)	2.16(2)	2.12(10)	3.19	3.15
HB										
deoxy	-	-	-	-	2.07(2)	2.07(2)	2.17(2)	2.21(2)	3.21	3.23
carboxy	1.78(1)	1.72(3)	2.91(3)	2.87(5)	2.01(1)	2.01(1)	2.04(2)	2.11(3)	3.15	3.17
oxy	1.89(2)	1.91(19)	3.01(2)	2.98(16)	2.03(1)	2.03(3)	2.15(2)	2.12(11)	3.17	3.19

^aXAS data refer to mean values from EXAFS at 20/260 K in Fig. S4 (full range of deviation from mean value in parenthesis). XRD (X-ray crystallography) values correspond to two (**deoxy**), four to five (**carboxy**), or four to five (**oxy**) structures for MB/HB in the protein data base (PDB) at better than 1.7 Å resolution (PDB entries 2DN2, 3QM6, 3RGK, 1A6M, 3QM7, 3E55, 1A6G, 4ESA, 1J40, 4HRR, 1IRD, 3A0G, 1LTW, 5HAV, 1MBO, 1MBD, 2Z6S, 1HBI, 2R80, 1THB, 2DN1, 1A6M; standard deviation in parenthesis).

Table S3: Bond lengths/angles and Mulliken spin densities in porphyrins/hemes from DFT.^a

		bond length [Å]				angle [°]	Mulliken spin		
		Fe- N _{porphyrin}	Fe- N _{His} /N,O,Cl	Fe- C/O(=O)	Fe (-C/O)=O	Fe- C/O=O	Fe	axial ligands	porphyrin
Porphyrin									
1 LS Fe(II)		2.01(2)	2.01(1)	-	-	-	0	0	0
2 HS Fe(II)		2.08(2)	2.32(1)	-	-	-	3.84	0.02	0.03
3 HS Fe(III)		1.99(3)	2.29(1)	-	-	-	4.16	0.23	0.11
heme									
deoxy		2.10(3) [2.07]	2.18(1) [2.18]	-	-	-	3.85(3)	-0.03(1)	0.04(2)
carboxy		2.03(2) [2.01]	2.09(1) [2.07]	1.79(1) [1.79]	2.93(1) [2.94]	177(1)	0	0	0
oxy	Pauling	2.05(6)	2.06(1)	1.75(1)	2.68(1)	122(1)	0	0	0
	Weiss	2.04(6) [2.04]	2.05(1) [2.16]	1.89(2) [1.91]	2.79(2) [3.02]	120(1)	1.12(2)	-1.01(2)	-0.03(1)

^aValues in parenthesis represent bond length and angle ranges within a given model (porphyrin compound and globin-heme structures) and for slight starting structure variations in the geometry-optimization (globin-heme structures), axial ligands include the CO/O₂ and bound histidine (His) ligands for the hemes, values in brackets show mean bond lengths at 20/260 K for MB/HB heme species from EXAFS (Table S2) for comparison. In the Pauling model for **oxy** the Fe-O₂ bond length was restraint to the value for the energetic minimum. Porphyrin compounds: **1**, Fe(TPP)(Py)₂; **2**, Fe(TPP)(THF)₂; **3**, Fe(TPP)Cl; TPP = tetraphenylporphyrin, Py = pyridine, THF = tetrahydrofuran.

Table S4(A): Natural orbitals in active space from CASSCF calculations.^a

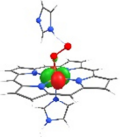
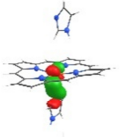
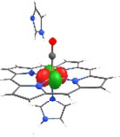
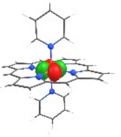
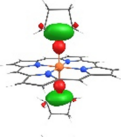

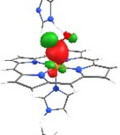
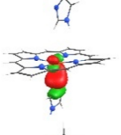
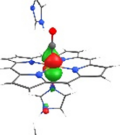
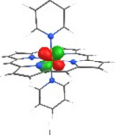
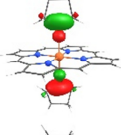
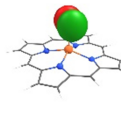
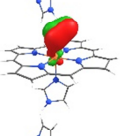
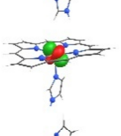
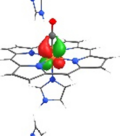
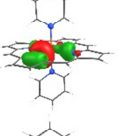
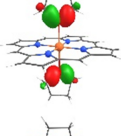
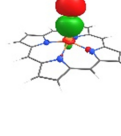
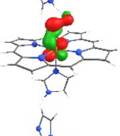
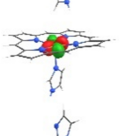
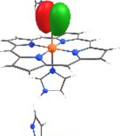
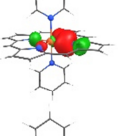
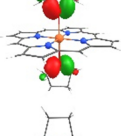
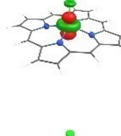
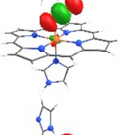
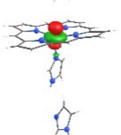

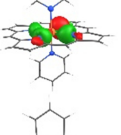
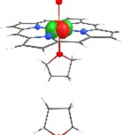
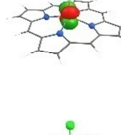
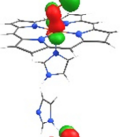
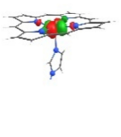
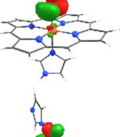
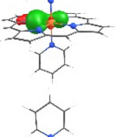
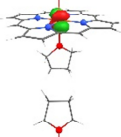
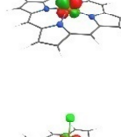
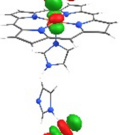


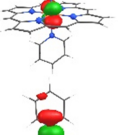
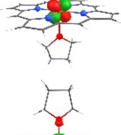
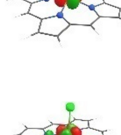
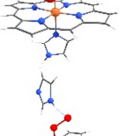


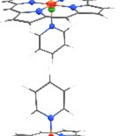
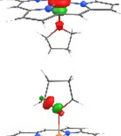
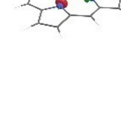
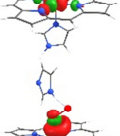


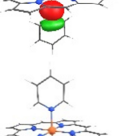
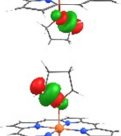

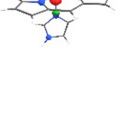


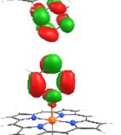
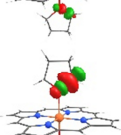




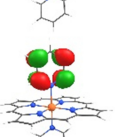
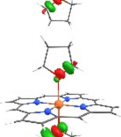




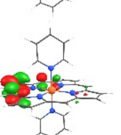








(A) MO no.	globin-heme			porphyrin compound		
	oxy	deoxy	carboxy	1 Fe(II) LS	2 Fe(II) HS	3 Fe(III) HS
1						
2						
3						
4						
5						
6						
7						
8						
9						
10						
11						
12						
13						

Table S4(B): Natural orbitals in active space from CASSCF calculations.^b

(B) oxy MO no.	Fe-O ₂ bond length [Å]					
	1.70	1.75	1.80	1.85	1.90	1.95
1						
2						
3						
4						
5						
6						
7						
8						
9						
10						

^aMOs for **oxy** in (A) correspond to a structure with an Fe-O₂ bond length of 1.875 Å (energy minimum); MOs were drawn at a contour level of 0.05. ^bMOs in (B) are for CASSCF (12,10) calculations for **oxy** after geometry-optimization of structures with an increasing (and fixed) Fe-O₂ bond length. For corresponding CASSCF parameters see Tables S5, S6 and Fig. S20.

Table S5: Summary of CASSCF calculations with active spaces shown in Table S4.

(A) ^a	heme			porphyrin		
	oxy	deoxy	carboxy	1 Fe(II) LS	2 Fe(II) HS	3 Fe(III) HS
	MO occupancy (state contribution to wavefunction in %)					
CASSCF states	2222220000 (62.2) 2222202000 (30.4) 2212121100 (1.1)	221111 (100)	22222200 (95.6) 22221111 (1.9) 22222020 (1.2) 22220202 (1.2)	222220 (99.7)	222211110000 (95.4)	22211111 (100)
MO no.	spin density					
1	1.980	2.000	2.000	2.000	1.978	2.000
2	1.975	2.000	2.000	2.000	1.978	2.000
3	1.974	1.000	2.000	2.000	1.976	2.000
4	1.972	1.000	1.955	2.000	1.976	1.000
5	1.950	1.000	1.955	2.000	1.000	1.000
6	1.332	1.000	0.045	2.000	1.000	1.000
7	0.706		0.045	2.000	1.000	1.000
8	0.051			2.000	1.000	1.000
9	0.034			2.000	0.023	
10	0.024			0.000	0.023	
11				0.000	0.023	
12				0.000	0.023	
13				0.000		

(B) oxy	occupancy	Fe-O ₂ bond length [Å]					
		1.700	1.750	1.800	1.850	1.900	1.950
MO no.	1 2 3 4 5 6 7 8 9 10	contribution to wavefunction [%]					
CASSCF states	2 2 2 2 2 2 0 0 0 0	68.8	66.4	64.2	62.2	60.3	58.6
	2 2 2 2 0 2 0 0 0 0	23.2	25.8	28.2	30.4	32.4	34.1
	2 2 1 2 1 2 1 1 0 0	1.3	1.2	1.1	1.1	1.1	1.1
	2 2 2 2 0 2 0 2 0 0	0.8	0.8	0.8	0.7	0.7	0.7
	2 2 1 2 1 1 2 1 0 0	0.6	0.6	0.6	0.6	0.7	0.7
	1 2 2 1 2 2 1 0 1 0	0.0	0.0	0.0	0.6	0.6	0.6
		spin density					
MO no.	1	1.981	1.981	1.981	1.980	1.980	1.979
	2	1.974	1.974	1.975	1.975	1.976	1.976
	3	1.970	1.972	1.973	1.974	1.974	1.975
	4	1.968	1.970	1.972	1.972	1.973	1.972
	5	1.948	1.949	1.950	1.950	1.951	1.951
	6	1.498	1.445	1.396	1.352	1.312	1.277
	7	0.542	0.594	0.643	0.687	0.726	0.762
	8	0.053	0.052	0.052	0.051	0.051	0.051
	9	0.036	0.035	0.034	0.034	0.034	0.035
	10	0.029	0.027	0.026	0.024	0.024	0.023
		effective unpaired electron density					
atom	Fe	1.760	1.907	1.927	1.988	2.036	2.078
	O1	0.326	0.256	0.302	0.298	0.294	0.292
	O2	0.000	0.000	0.000	0.000	0.000	0.000

^aData in (A) correspond to CASSCF calculations on geometry-optimized structures with the following parameters; species/(electrons,MOs): **oxy**/(12,10), **deoxy**/(8,6), **carboxy**/(10,7), porphyrin **1**/(18,13), porphyrin **2**/(12,12), porphyrin **3**/(11,8). ^bData in (B) stem from CASSCF (12,10) calculations for geometry-optimized **oxy** structures with a fixed Fe-O₂ bond length (O1/2 = atoms of O₂ bound/not bound to Fe). The following results were derived from the **oxy** calculations (for a ~1.9 Å Fe-O₂ bond at the energy minimum, see also Table S6). The wavefunction of **oxy** is dominated (~90 %) by two contributions, as observed earlier (35-37); all other configurations each contribute <2 %. The ratio of the two main configurations varies with the Fe-O₂ bond length and for a longer bond the relative contribution of configuration two is increased (see Fig. S20). Both configurations contain essentially unoccupied Fe(d_{z²}) and Fe(d_{x²-y²}) orbitals and a double-occupied MO (2), which represents a polarized σ(Fe-O) bond with dominant O(p) and weak Fe(d_{z²}) contributions, suggesting strong bond polarization (i.e. an ionic dative bond with few electron density transfer from O₂ to the Fe(d_{z²}) orbital) (37, 38). A further double-occupied MO (4) with dominant Fe(d_{xz}) and minor O(p) contributions is suggestive of further π-backbonding. Double-occupied MOs representing π(Fe-O) (6) and π*(Fe-O) (7) bonds show dominant Fe(d_{xz/yz}) and weaker O(p) contributions (with larger relative Fe(d) character in configuration one) and change between double and zero occupancy in the two configurations. The Takatsuka effective unpaired electron density (EUED) in MOs 6 and 7 each is ~0.9 and the total EUED on iron of ~2 results from ~90 % and ~10 % contributions from MOs 6-7 and 1, 4, 9, and 10. The total EUED on O₂ is ~0.3 so that the sum of iron and oxygen contributions is ~2.3. The latter value is close to the EUED for ozone (10). These findings indicate in effect two unpaired spins on iron, which were experimentally observed in our Kβ emission analysis, and thus a formal intermediate spin state, significant double-bond character of the Fe-O₂ interaction, bonding electron delocalization over the three atoms, and limited charge transfer to O₂ implying minor superoxide radical character of the ligand and a merely ferrous iron. The global picture of the Fe-O₂ bonding in MB/HB therefore converges towards a three-center interaction, which comprises certain features of each of the classical models. We note that the narrow-sense Pauling model with a canonical LS Fe(II) and neutral O₂ ligand is excluded in particular by our Kβ main-line data, which clearly reveal a higher spin state of iron in **oxy**.

Table S6: AO contributions to MOs from CASSCF for oxy.^a

oxy		atom																
		Fe								O1				O2				
MO no.	energy [eV]	AO contribution [%]																
		s	p	d					s	p			d	s	p			d
				z^2	x^2-y^2	xz	yz	xy		z	x	y			z	x	y	
1	-18.8	2	0	3	0	0	0	91	0	1	0	1	0	0	0	0	0	0
2	-17.1	1	3	9	0	3	1	4	7	47	9	10	0	0	1	1	0	2
3	-15.9	0	0	0	0	3	7	0	0	2	19	32	1	0	0	11	22	1
4	-17.0	0	0	0	0	44	41	0	0	3	1	5	0	0	0	1	3	0
5	-19.3	0	0	1	0	1	0	0	0	14	24	9	1	0	16	23	9	1
6	-7.2	0	0	0	0	26	27	0	0	0	4	9	1	0	0	10	21	0
7	-3.6	0	0	0	0	23	24	0	0	0	8	15	1	0	0	10	19	1
8	15.6	0	0	0	0	0	0	0	5	10	21	8	5	4	13	19	7	5
9	6.9	0	0	0	87	0	0	0	0	0	0	0	0	0	0	0	0	0
10	20.6	3	7	29	0	0	1	1	6	40	2	4	1	0	0	0	0	1

^aData refer to CASSCF (12,10) calculations (1.9 Å Fe-O₂ bond) in Tables 1, S4, and S5, O1 is the oxygen atom directly bound to Fe, O2 is the 2nd-sphere atom of O₂.

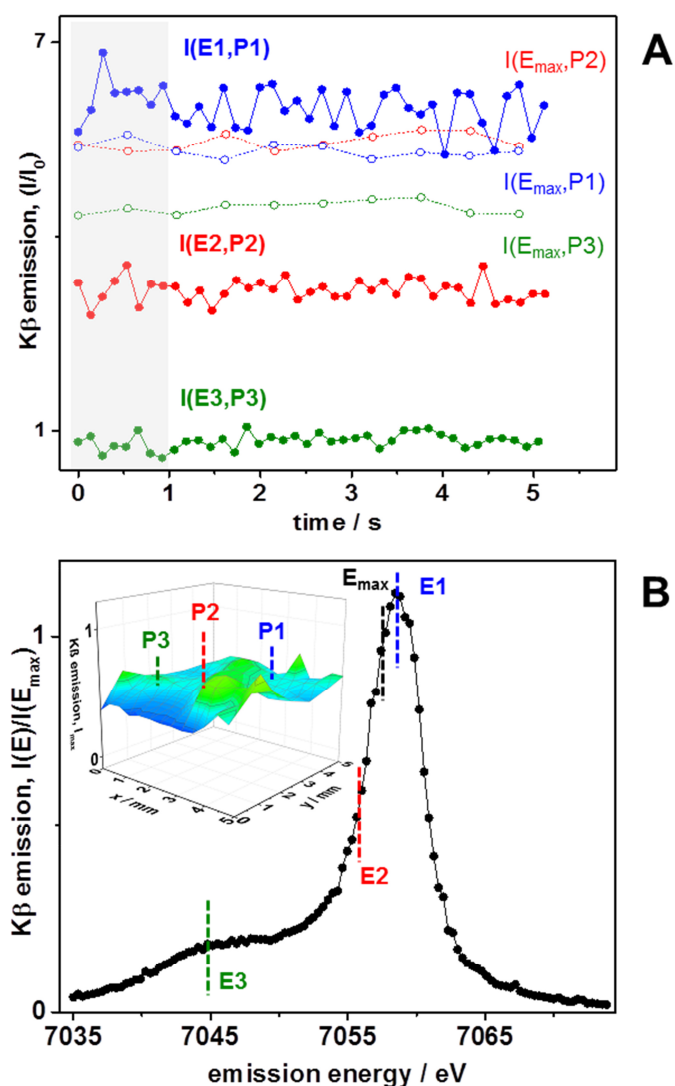


Figure S1: Time-resolved energy-sampling K β XES. (A) X-ray fluorescence (I) time traces at three energies (E1-3) in the K β main line region (solid symbols) and at a constant reference energy (open symbols) close to the K $\beta_{1,3}$ maximum (E_{\max}) at the same sample positions (P1-3) for an oxy HB sample at 260 K. (B) K β spectrum as derived from data as in (A) after dividing the mean $I(E_i, P_j)$ values of data points in the first second of the time traces (grey bar in A), each measured on a fresh sample spot, by the mean $I(E_{\max}, P_j)$ values corresponding to the mean value of data points in 0-5 s of the time traces (yielding a >2-fold better signal-to-noise ratio in the $I(E_{\max})$ reference data vs. the $I(E)$ data). The inset shows a ‘microscopic’ picture of the metal distribution in the sample from the emission counts, revealing moderate thickness variations of the frozen solution in the x-y area used for collection of a complete K β spectrum and approximate positions used for collection of data in (A). K β satellite emission spectra were collected using the same energy-sampling approach. For the spectra in Figs. 2 and 5, data points within a time window of 0-1 s at each emission energy were averaged and up to 10 data sets for the hole K β main- and satellite-line emission energy ranges were averaged.

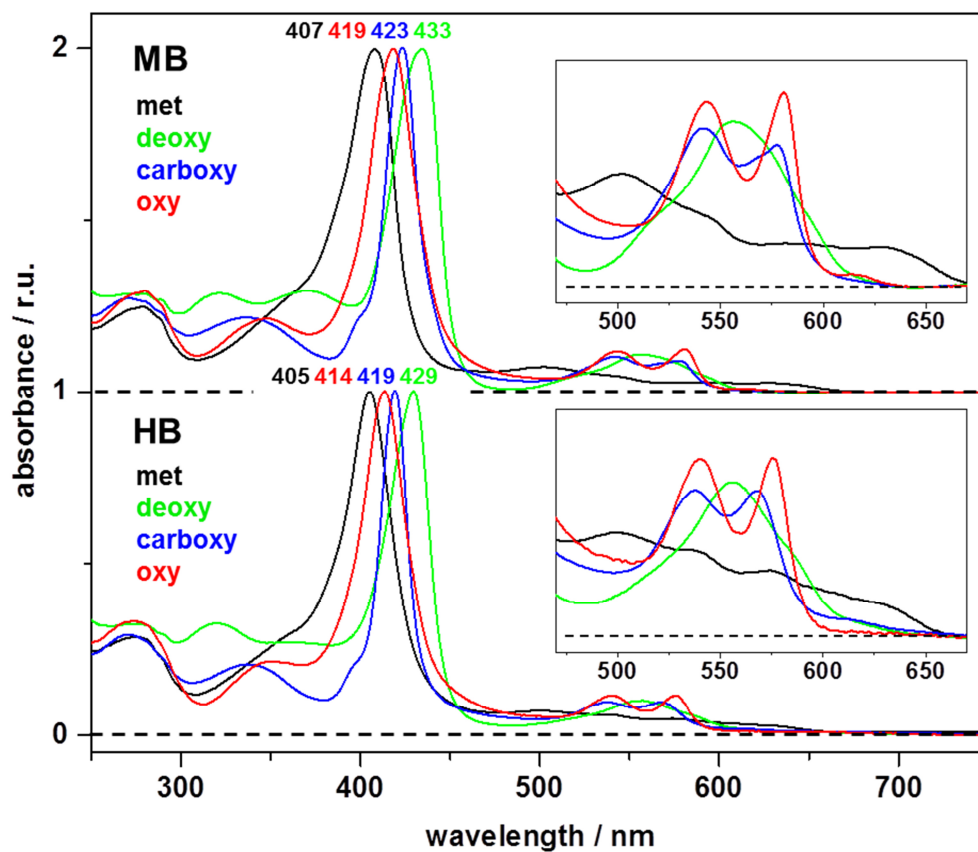


Figure S2: Optical absorption spectra of MB and HB. Spectra were normalized at the Soret band amplitudes at the indicated wavelengths. Insets: magnification of spectra in the Q-band region. Spectra correspond to aliquots ($\sim 12 \mu\text{M}$) of HB/MB protein preparations for XAS/XES in buffer solutions under N_2 (**met/deoxy**) or CO/O_2 (**carboxy/oxy**) atmospheres.

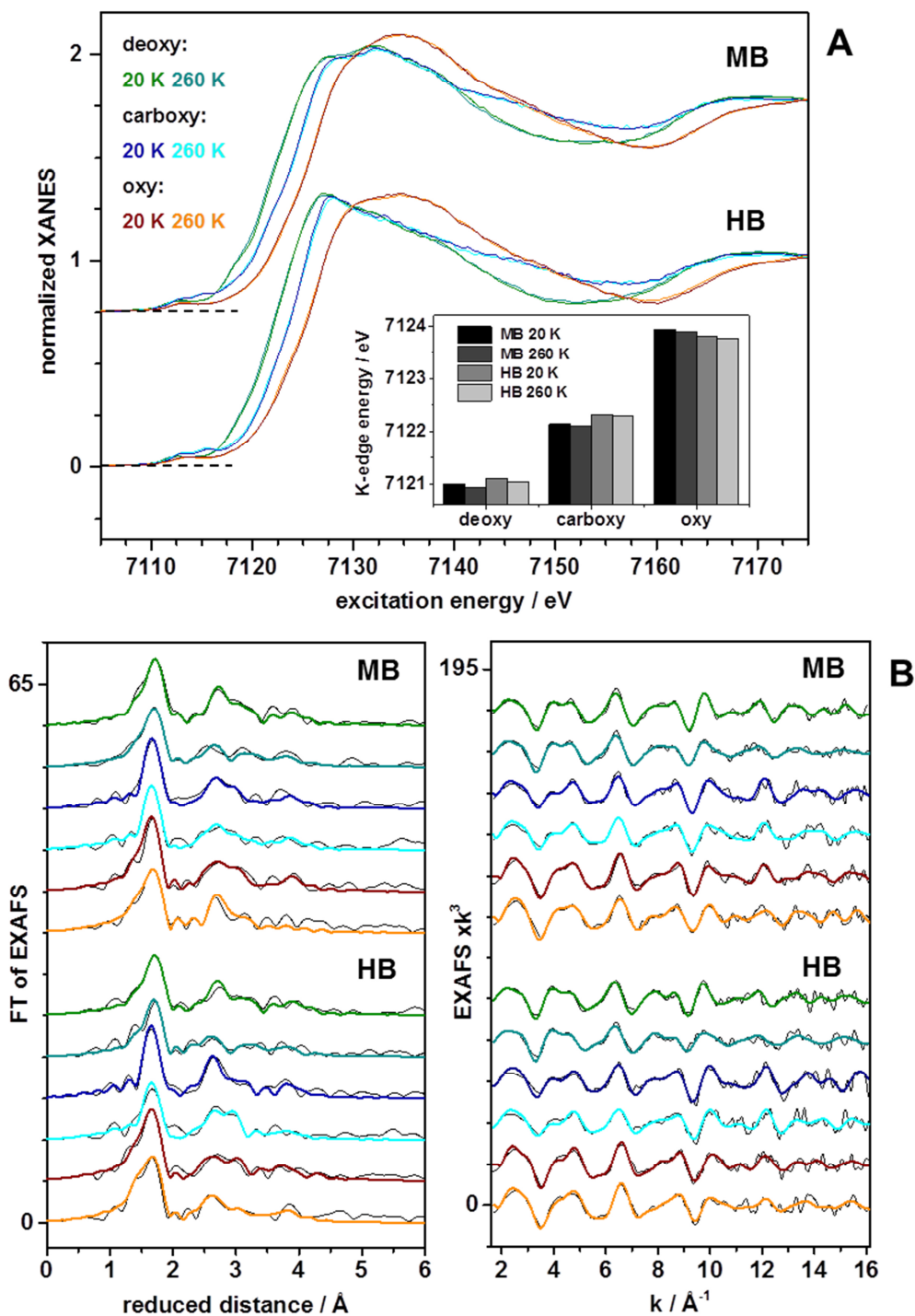


Figure S3: Lower-resolution XANES and EXAFS spectra of MB and HB at 20 K and 260 K. (A) XANES spectra of MB/HB (vertically shifted) and respective K-edge energies at 50 % level in the inset. (B) EXAFS spectra (left, Fourier-transforms calculated for k -values of 1.6–16.2 \AA^{-1} with cos windows extending over 10 % at each k -range end, and right, corresponding EXAFS oscillations; black lines, experimental data; colored lines, simulations with parameters in Fig. S4).

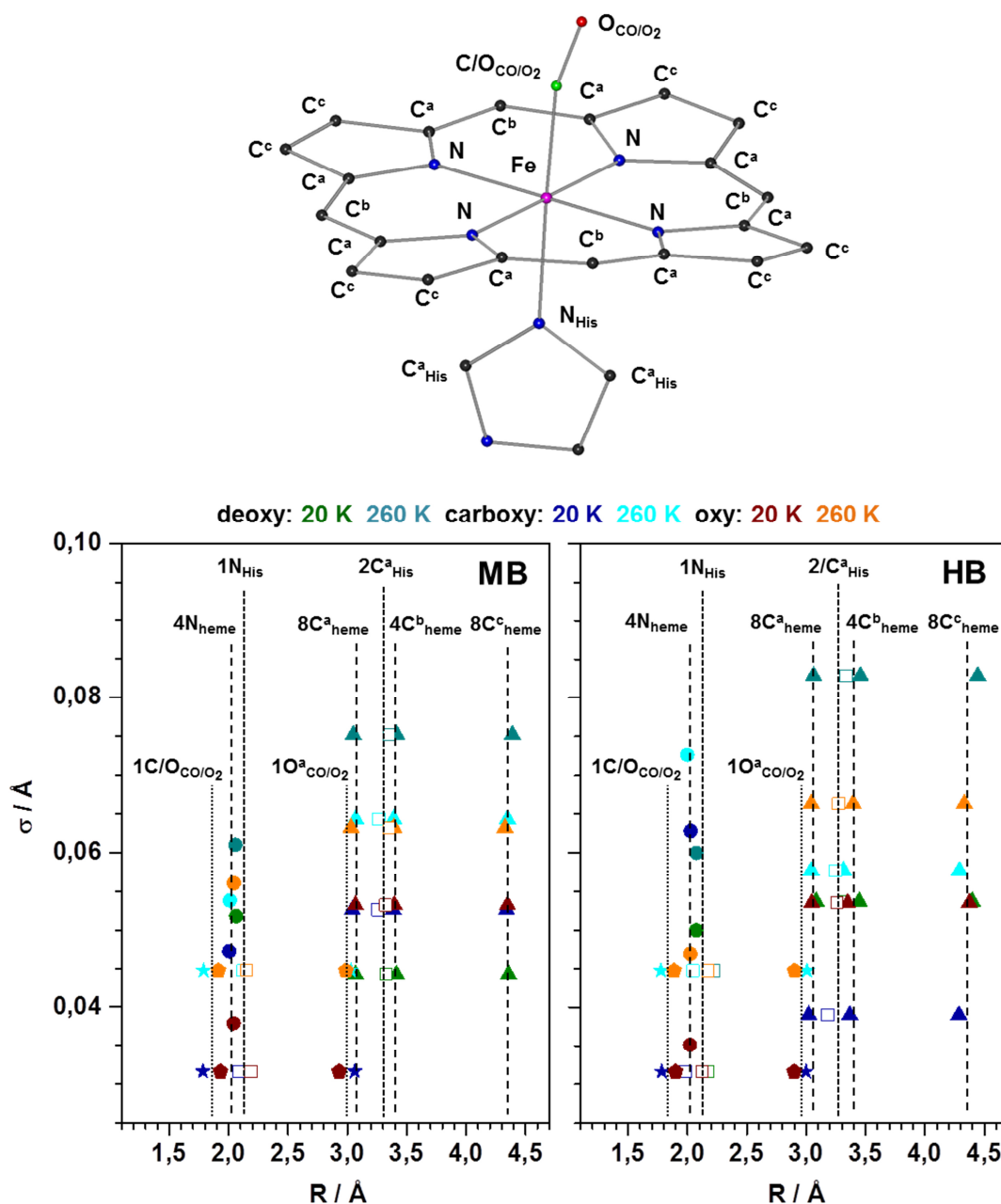


Figure S4: Interatomic distances from EXAFS analysis. Top: schematic heme structure with marked atoms in the 1st, 2nd, and 3rd coordination spheres of the iron center in **deoxy**, **carboxy**, and **oxy**. Bottom: EXAFS fit results corresponding to spectra at 20/260 K in Fig. S3 (R , interatomic distance; σ , Debye-Waller parameter; numbers in the annotations of the vertical lines represent coordination numbers, N , as used in the fits). Vertical lines were drawn at respective mean distances to emphasize similarities for MB/HB at 20/260 K. Interatomic distances from EXAFS and crystal structures are compared in Table S2.

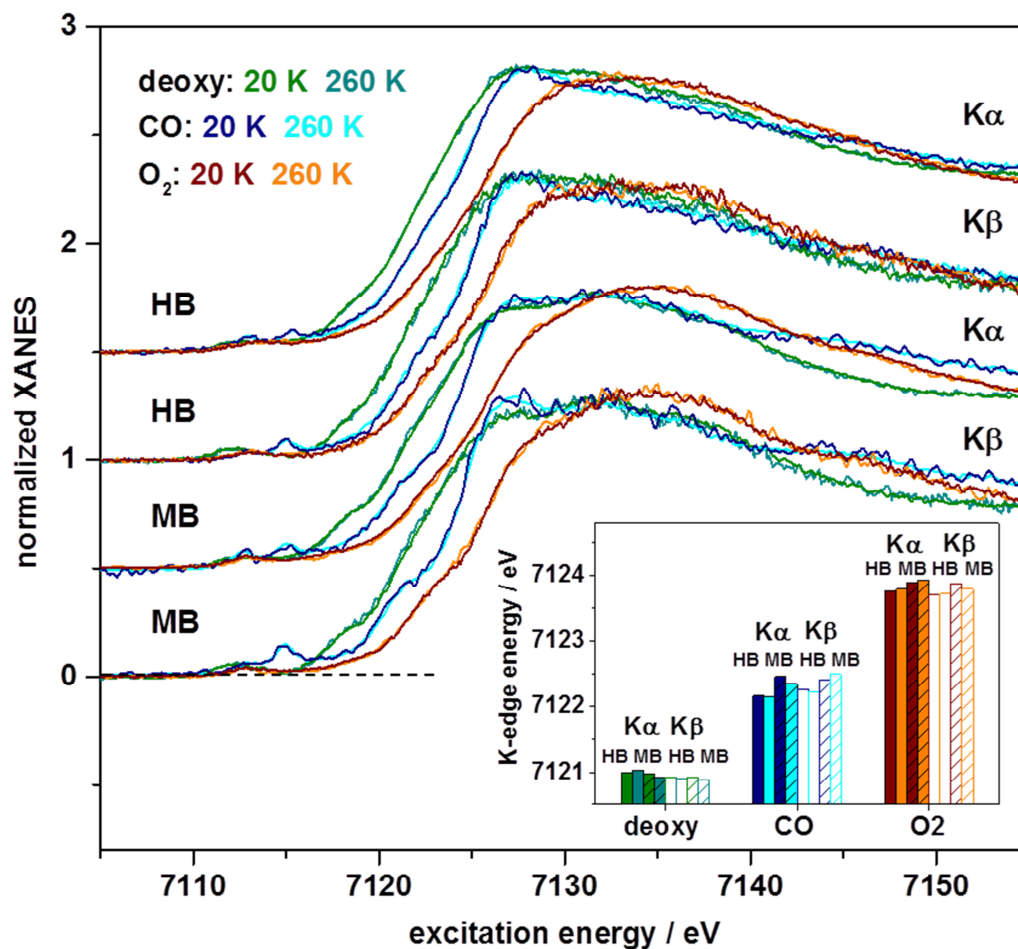


Figure S5: Higher-resolution XANES spectra of MB and HB. Spectra of the three heme species at 20/260 K (vertically shifted) were collected using a Si[311] double-crystal monochromator and broad-band (~ 150 eV, “total-fluorescence”) $K\alpha$ detection or narrow-band (~ 1 eV) $K\beta$ emission detection (at energies at the maximum of the respective $K\beta_{1,3}$ emission line, see Fig. 2). The inset shows respective K-edge energies (at 50 % level). Note within noise limitations similar K-edge energies for both detection methods, which are also similar to the data in Fig. S3A.

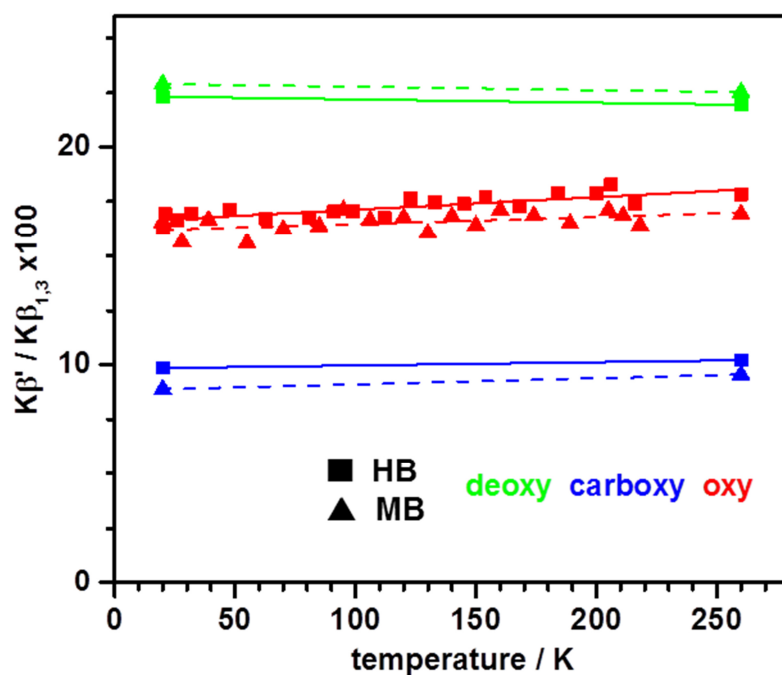


Figure S6: Temperature-independence of $K\beta$ line ratios in MB and HB. For the three heme species, intensity ratios at 20 K and 260 K correspond to main-line emission amplitudes at 7045 eV ($K\beta'$) and the $K\beta_{1,3}$ maximum of non-resonantly excited spectra in Fig. 2. For **oxy**, the further data points were derived from absolute emission intensities at 7045 eV ($K\beta'$) and 7057 eV ($K\beta_{1,3}$), which were measured (0.5 s acquisition) on separate sample spots during stepwise lowering of the temperature from 260 K to 20 K and amplitude normalized to the mean 20/260K intensity ratios. Lines show linear fits to the data points (dashed lines, MB; solid lines, HB). Slight apparent line slopes result from minor inaccuracies in the count rate normalization due to sample thickness variations (Fig. S1) in this type of experiment and are not related to iron spin state changes within the 20-260 K temperature range.

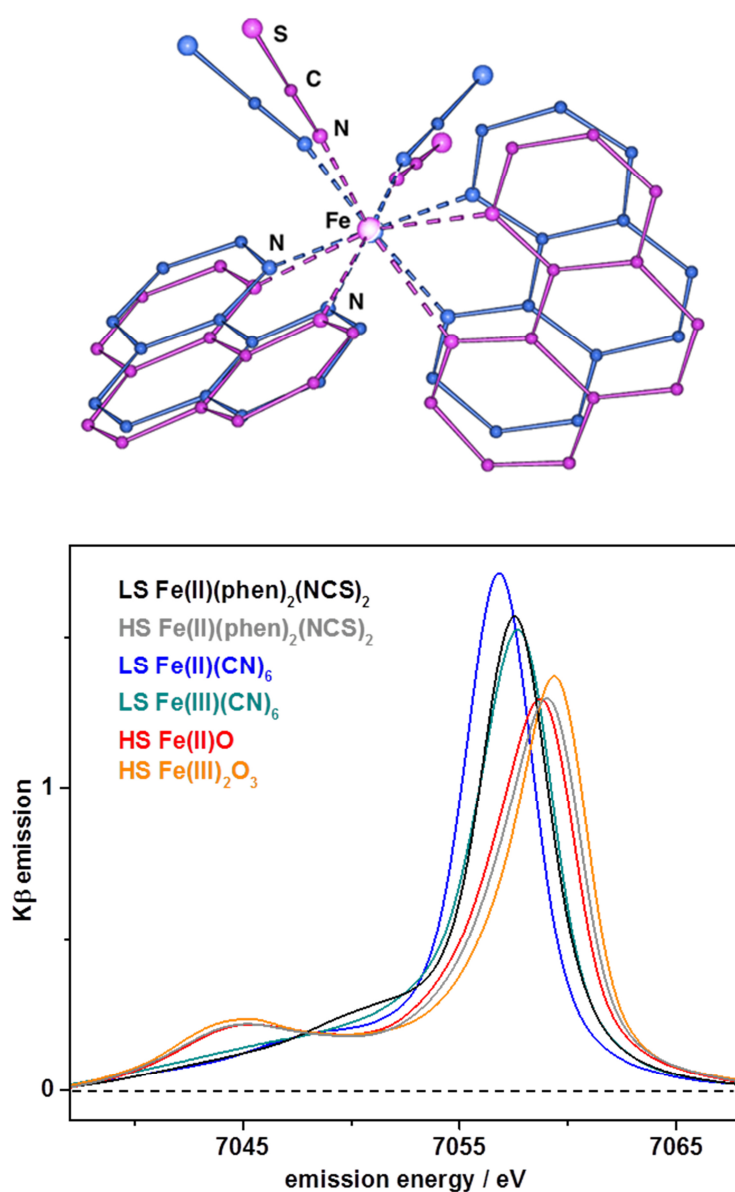


Figure S7: Structures and K β spectra of non-porphyrin compounds. Top: Superposition of crystal structures of Fe(II)(phen)₂(NCS)₂ (phen = 1,10-phenanthroline) at 130 K (low-spin state, blue) and 293 K (high-spin state, magenta), see ref. (1) for details. The structures of the octahedral iron centers in Fe(II/III)(CN)₆ and in the HS iron oxides are available in the Cambridge Structural Database (CSD). Bottom: Spectra of microcrystalline (powder) materials of the indicated oxide or cyanide complexes and of the molecular compound were normalized and measured at 20 K, except of the spectrum of HS Fe(II)(phen)₂(NCS)₂ showing abrupt and complete spin crossover (LS \rightarrow HS transition) at \sim 175 K (1), which was measured at 260 K.

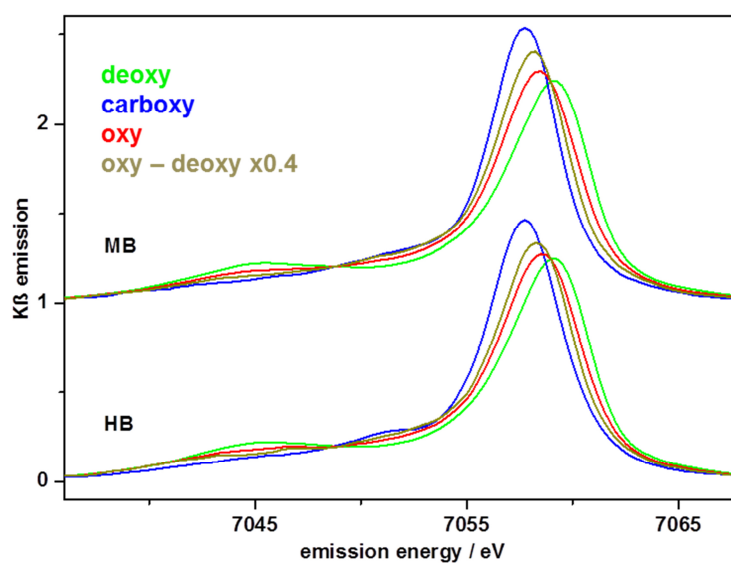


Figure S8: Purity of $K\beta$ spectra of **oxy** MB/HB. Mean spectra at 20/260K for the three heme species are compared to (re-normalized) spectra of **oxy** after subtraction of 40 % of the **deoxy** spectra. This procedure resulted in distorted line shapes (i.e. in the $K\beta'$ region) and a respective large **deoxy** contribution was excluded based on the UV/vis and XAS data.

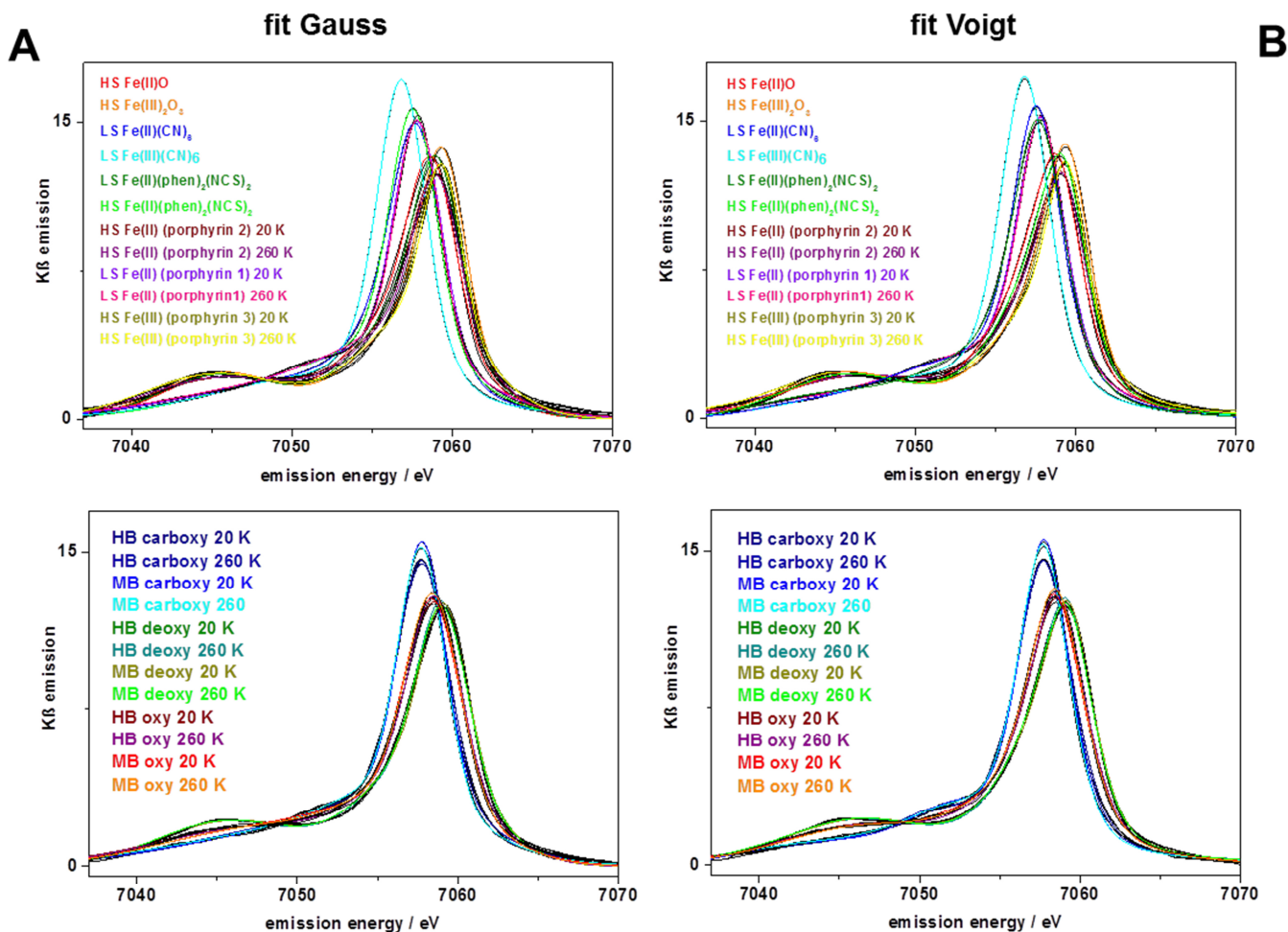


Figure S9: Fit analysis of K β main-line spectra. Top panels: spectra of porphyrin and non-porphyrin compounds. Bottom panels: spectra of MB and HB. (A) Experimental spectra (black lines) and fits with three Gaussian functions with variable band widths (colored lines). (B) Experimental spectra (black lines) and fits with three Voigt functions with variable band widths (50 % Gaussian and Lorentzian characters) and a linear baseline.

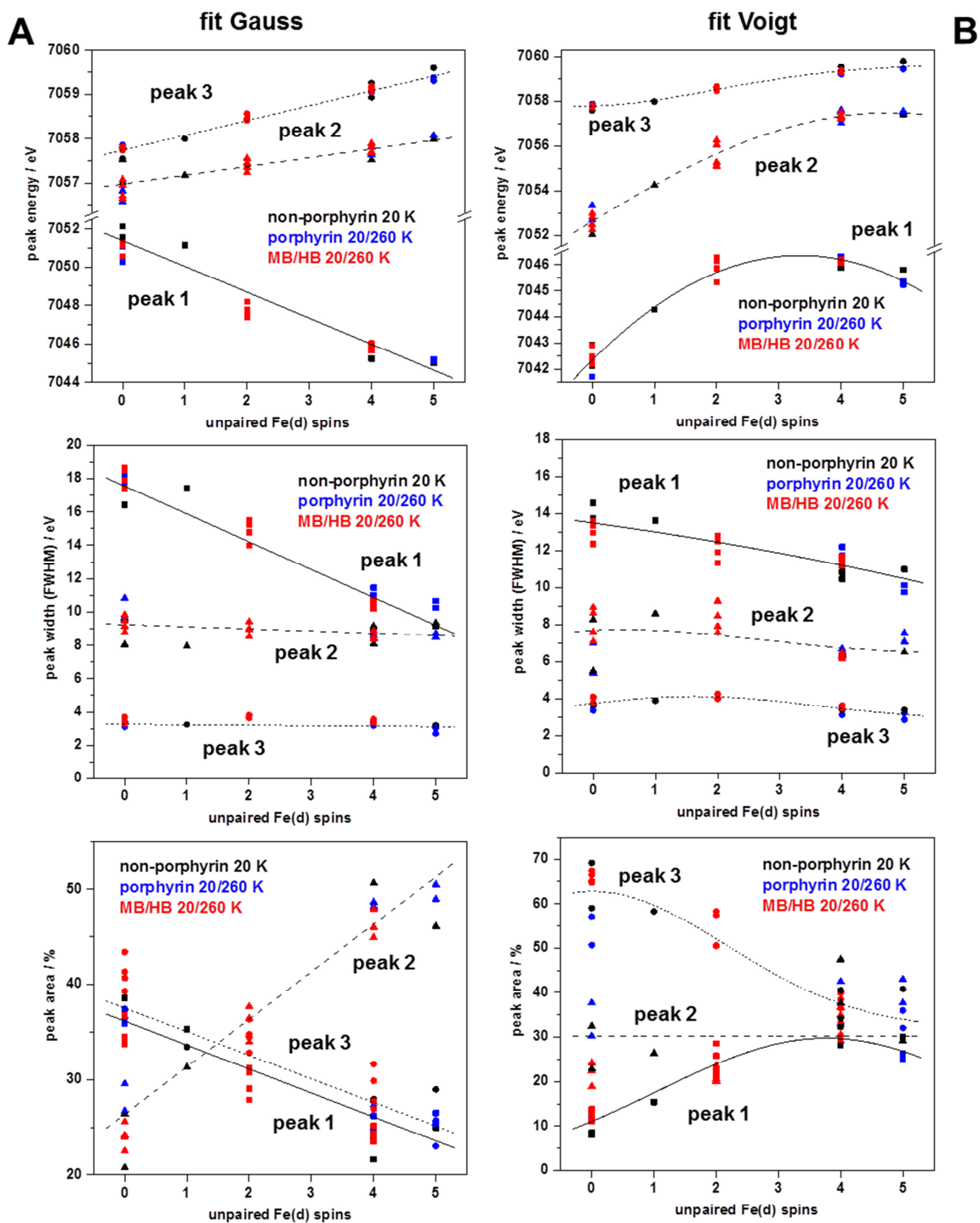


Figure S10: Fit results of K β spectra. Data correspond to fit curves in Fig. S9. Left: data from fits with Gaussian functions. Right: data from fits with Voigt functions. Top panels, line peak energies; middle panels, peak widths; bottom panels, integral peak areas. Lines show linear fits (left panels) or Gaussian fits (right panels) to the data for guiding the eye. Heme species in MB/HB were placed at Fe(d) spin counts of 4 (**deoxy**), 0 (**carboxy**), or 2 (**oxy**).

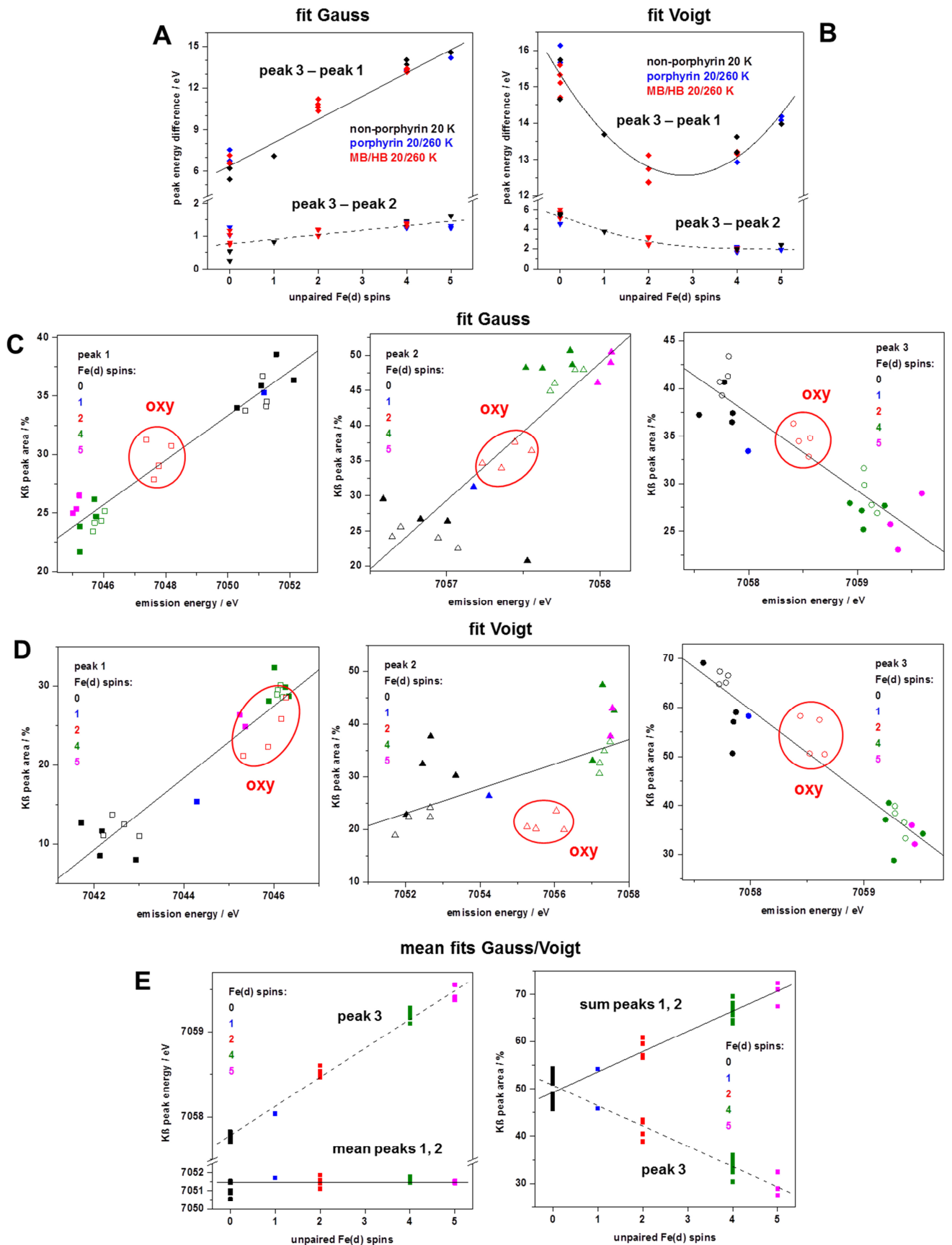


Figure S11: Correlations from K β fit analysis. Data correspond to Figs. S9 and S10. (A and B) K β line energy differences (lines show linear, left, or Gaussian, right, fits). (C and D) K β

peak areas vs. center energies (lines show linear fits) for the indicated (formal) number of unpaired Fe(d) spins in the porphyrin/non-porphyrin compounds and HB/MB; data for **oxy** (red circles) was placed at a Fe(d) spin count of 2. (E) Combined $K\beta$ peak energies (mean (left) or sum (right) of peaks 1/2 and peak 3) plotted vs. unpaired Fe(d) spin counts (lines show linear fits). The combined Gauss/Voigt data reproduce relative energies/intensities of $K\beta'/K\beta_{1,3}$ features as obtained from visual inspection of $K\beta$ spectra or $K\beta'$ amplitude determination (Figs. 2, 3).

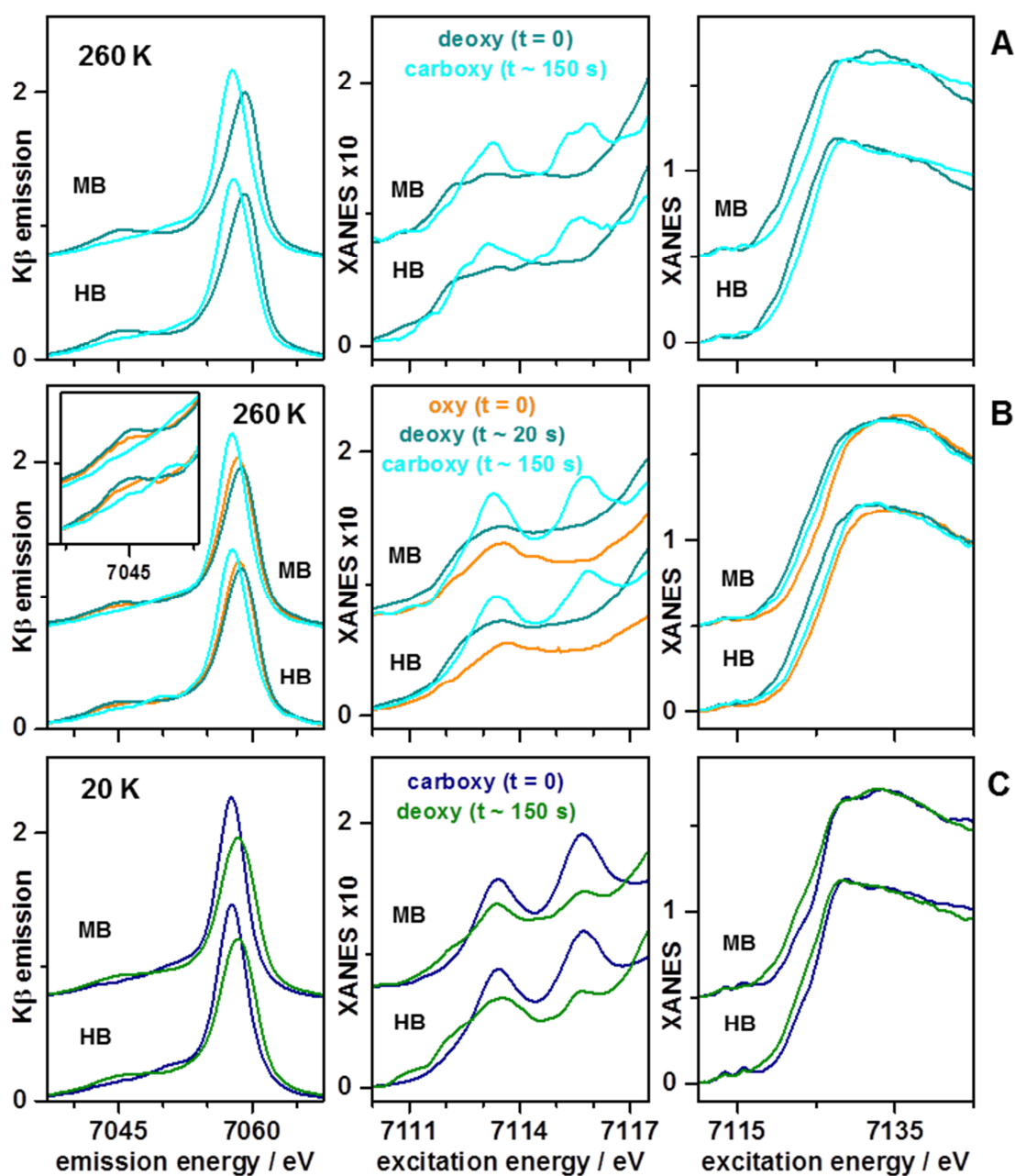


Figure S12A,B,C: X-ray induced species modifications. Spectra (left, $K\beta$ main lines; middle, pre-edge absorption; right, $K\alpha$ -detected XANES) were obtained at 260 K (A and B panels) or

20 K (C panels) for MB/HB containing the indicated initial heme species (at $t = 0$ corresponding to ~ 1 s of X-ray exposure, see Figs. 2, 4, and S5) or after $\sim 20/150$ s of irradiation, i.e. close to the completion of X-ray induced apparent conversion of **deoxy** to **carboxy** (top), of **oxy** first to **deoxy** and then to **carboxy** (middle), or of **carboxy** to **deoxy** (bottom) (Fig. 4). Note, e.g., the increase of the $K\beta'$ feature followed by a decrease (B, left) when starting from **oxy**, which corroborates the virtual absence of a **deoxy** fraction in the **oxy** samples. The data indicate a reversible spin state transition LS Fe(II) \rightarrow HS (FeII) for **carboxy** \rightarrow **deoxy** upon ligand release/rebinding and a IS Fe(II) \rightarrow HS Fe(II) \rightarrow LS Fe(II) conversion when starting from **oxy**.

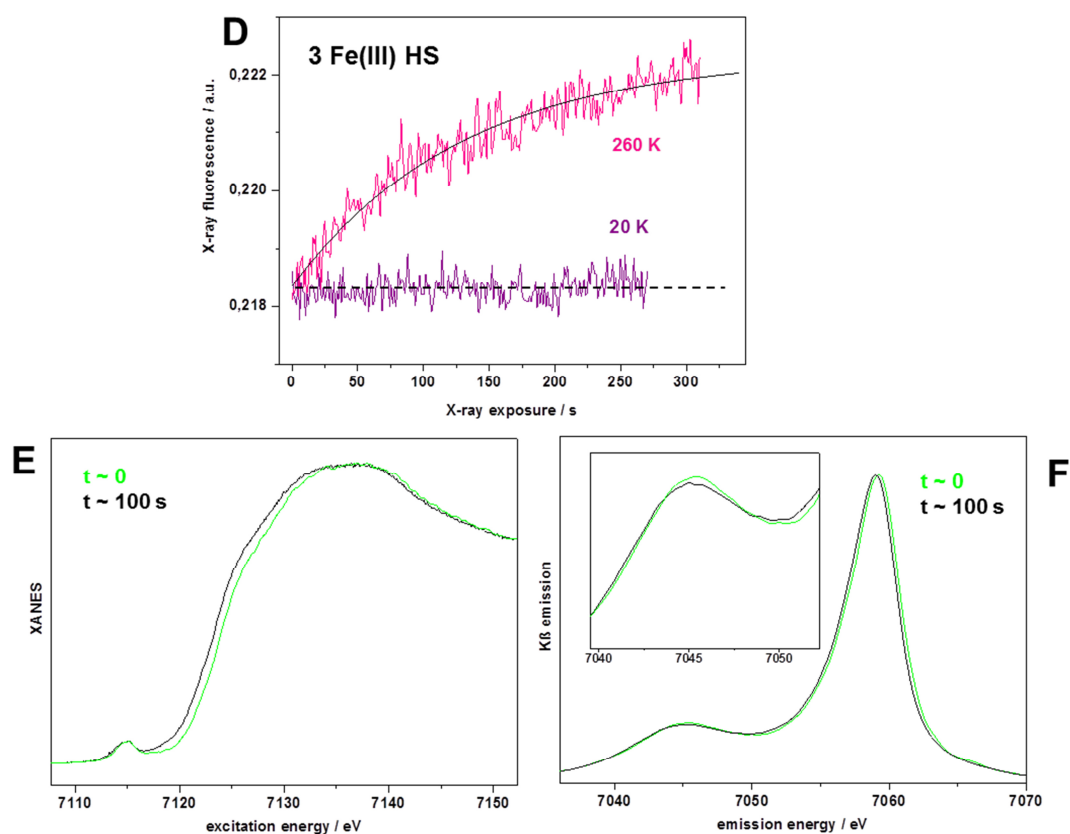


Figure S12D,E,F: X-ray induced species modifications. (D) X-ray fluorescence (at 7124 eV, arbitrary units) timescan data of porphyrin compound **3** show the absence of radiation induced Fe(III) reduction at 20 K within ~ 5 min of X-ray exposure and relatively slow and monophasic reduction of Fe(III) to Fe(II) at 260 K (the solid line shows a single-exponential fit). The mono-phasic (metal-centered) reduction of **3** is in contrast to the biphasic (ligand-centered) species modifications in the **carboxy** and **oxy** heme species (Fig. 4). (E) XANES spectra and (F) $K\beta$ main line emission spectra at ~ 0 s and ~ 100 s of X-ray exposure. Energy shifts of spectra indicate Fe(III) to Fe(II) reduction in **3**. Note the $K\beta'$ line decrease at ~ 100 s.

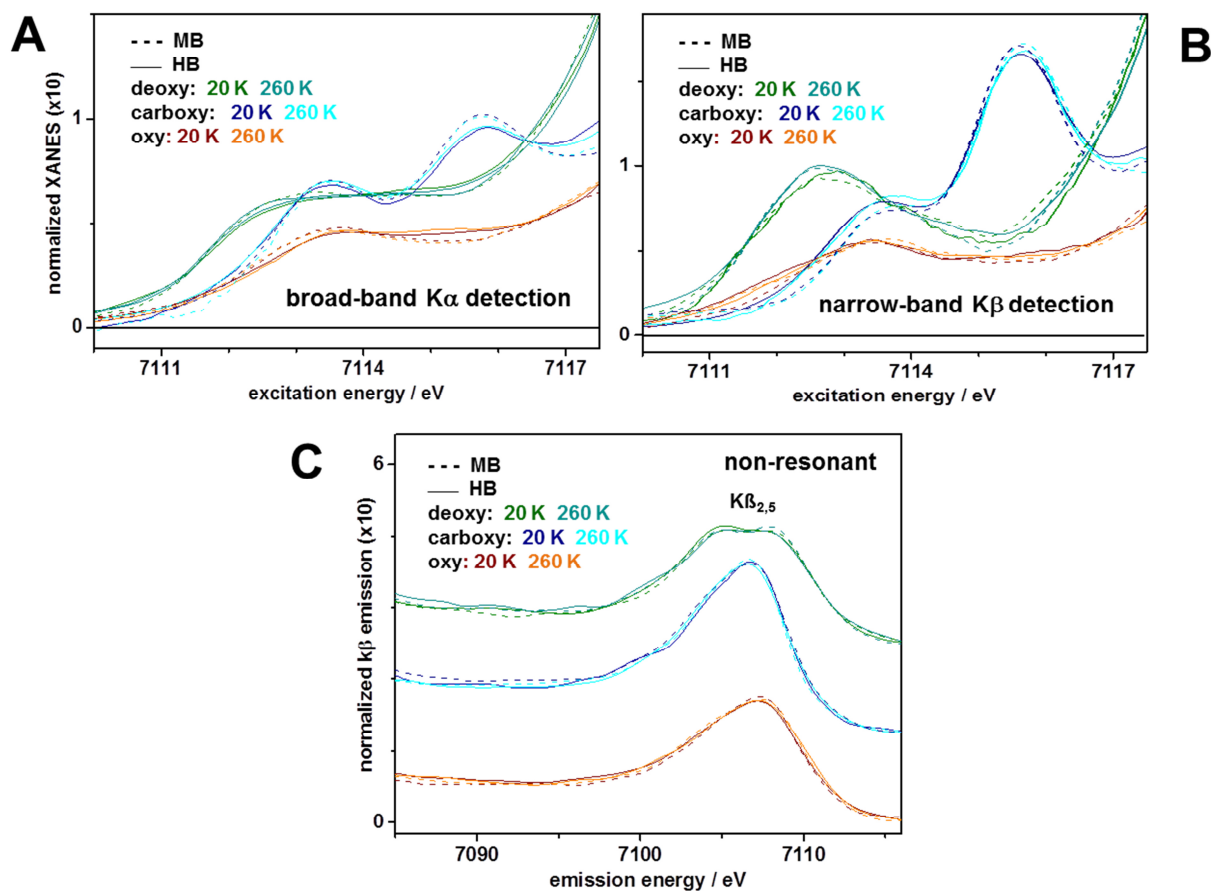


Figure S13: Pre-edge absorption (ctv) and K β satellite emission (vte) spectra of MB/HB. (A and B) Pre-edge absorption spectra at 20/260 K were measured (~ 1 s scan duration) at conditions similar to the XANES data in Fig. S5, but within a more narrow energy range (7109-7119 eV), and scaled to the respective XANES spectra. (C) K β satellite emission spectra at 20/260 K (vertically shifted) approximately normalized to the respective K β main-line spectra (Fig. 2). ctv/vte spectra in Fig. 4 were obtained after subtraction of smooth polynomial background curves due to the main K-edge rise (ctv) or the high-energy K $\beta_{1,3}$ tail (vte) from the spectra in (A) and (C) and area normalization of K β satellite emission spectra.

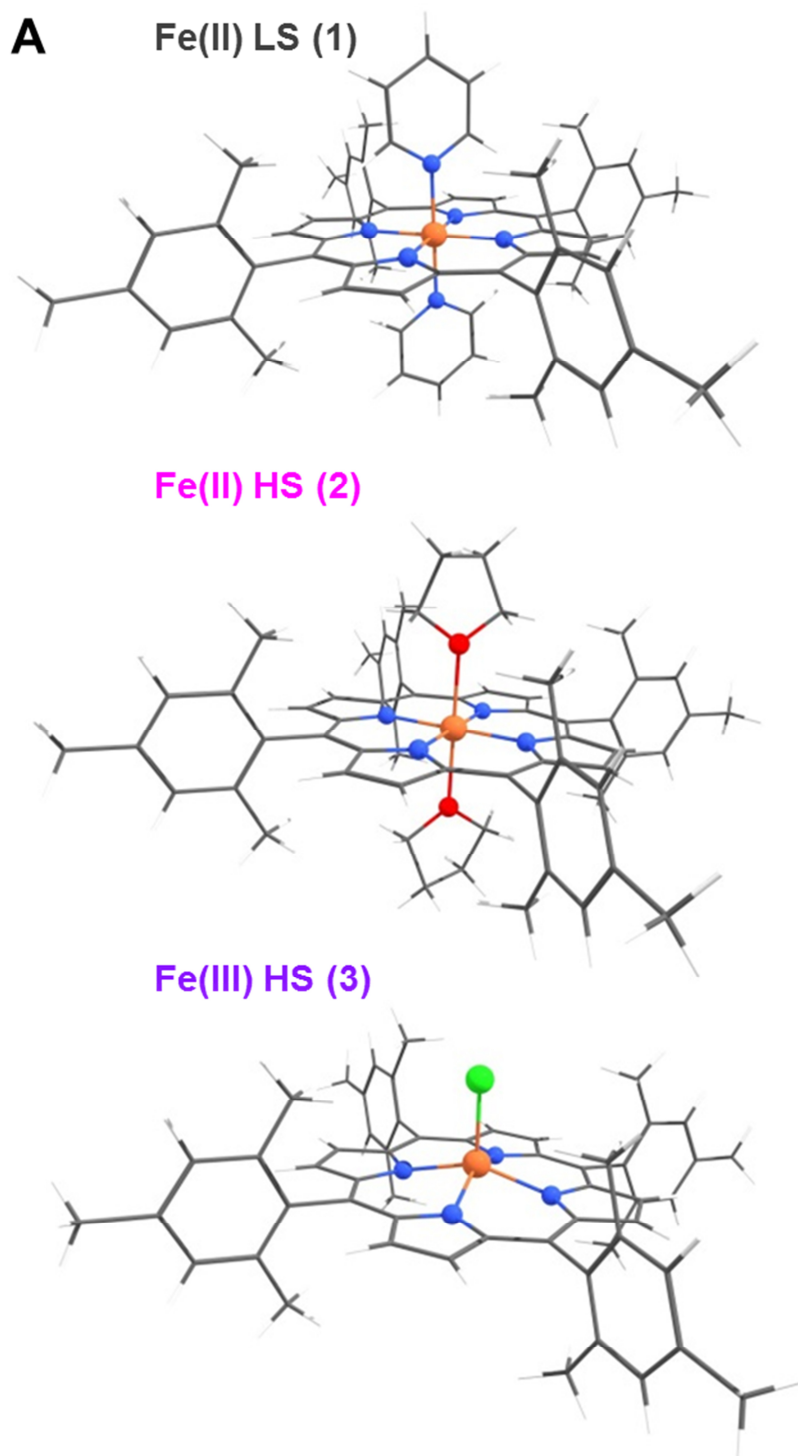


Figure S14A: Structures and XAS/XES data for porphyrin compounds. (A) Geometry-optimized crystal structure of **1** and geometry-optimized model structures of **2** and **3** from DFT (orange, Fe; blue, nitrogen; red, iron; green, chloride; grey, carbon). **1**, Fe(TPP)(Py)₂; **2**, Fe(TPP)(THF)₂; **3**, Fe(TPP)Cl (TPP = tetraphenylporphyrin, Py = pyridine, THF = tetrahydrofuran).

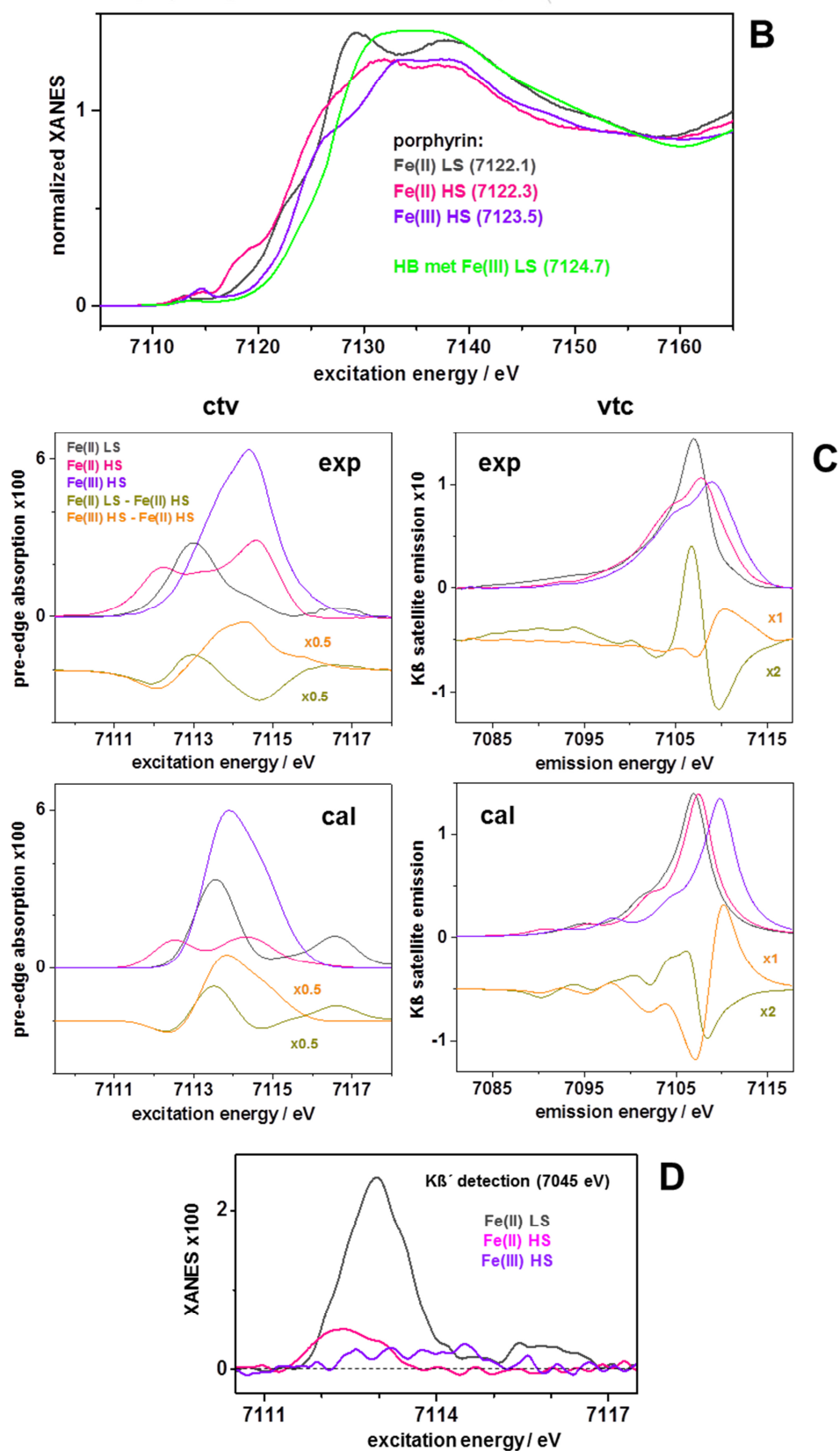


Figure S14B,C,D: Structures and XAS/XES data for porphyrin compounds. (B) High-resolution XANES spectra (Si[311] double-crystal monochromator, K α -fluorescence detection) of porphyrin compounds **1**, **2**, and **3** and of **met** HB (spectrum reproduced from ref.

(39)) and K-edge energies in eV in parenthesis. (C) Experimental (exp) background-corrected ctv (left) and vtc (right) spectra (top panels) for powder samples of **1-3** and calculated (cal) spectra from TDDFT (ctv) or DFT (vtc) (bottom panels) for geometry-optimized structures of **1-3**. Respective scaled difference spectra as indicated are shown for comparison (vertically shifted). (D) Narrow-band $K\beta'$ -detected (7045 eV) background-corrected ctv spectra of **1-3** (scaled to respective XANES spectra). Mean experimental spectra obtained at 20/260 K are shown in A-D.

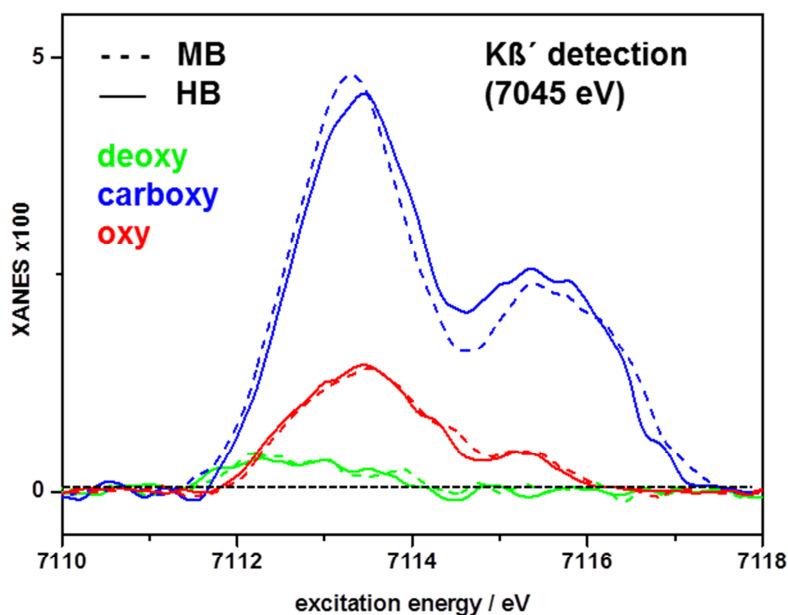


Figure S15: $K\beta'$ -detected ctv spectra of MB/HB. Background-corrected spectra of the three heme species represent the mean of data obtained at 20/260 K for 7045 eV emission detection and were scaled to the respective XANES spectra.

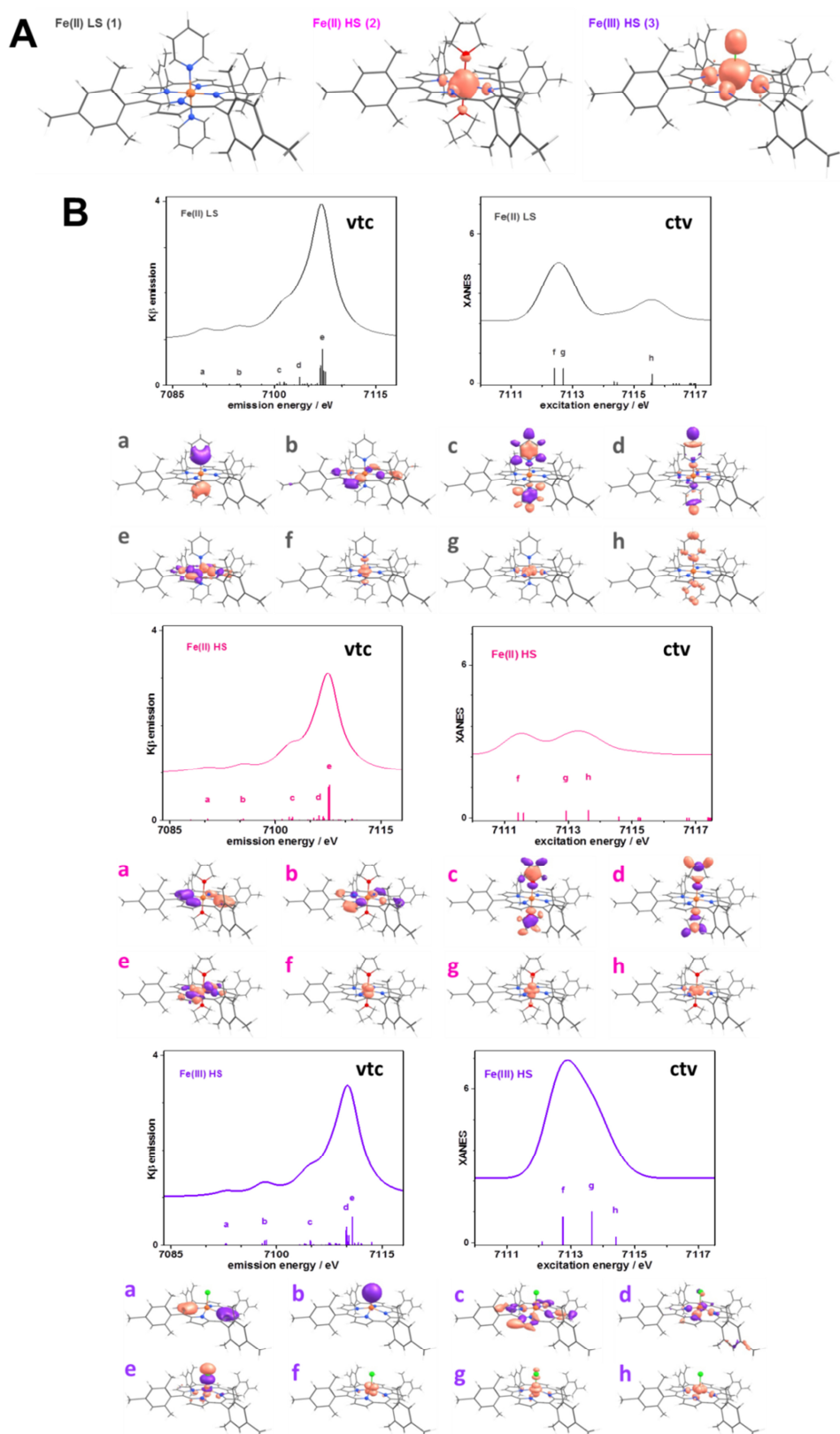


Figure S16: Spin densities and target/source MOs for ctv/vtc transitions in porphyrins. (A) Spin density distributions from DFT for the three porphyrins. (B) Calculated ctv (right) and vtc (left) spectra after broadening of stick spectra (top panels) and target/source MOs for selected electronic ctv excitation (a-e) and vtc decay (f-h) transitions (bottom panels).

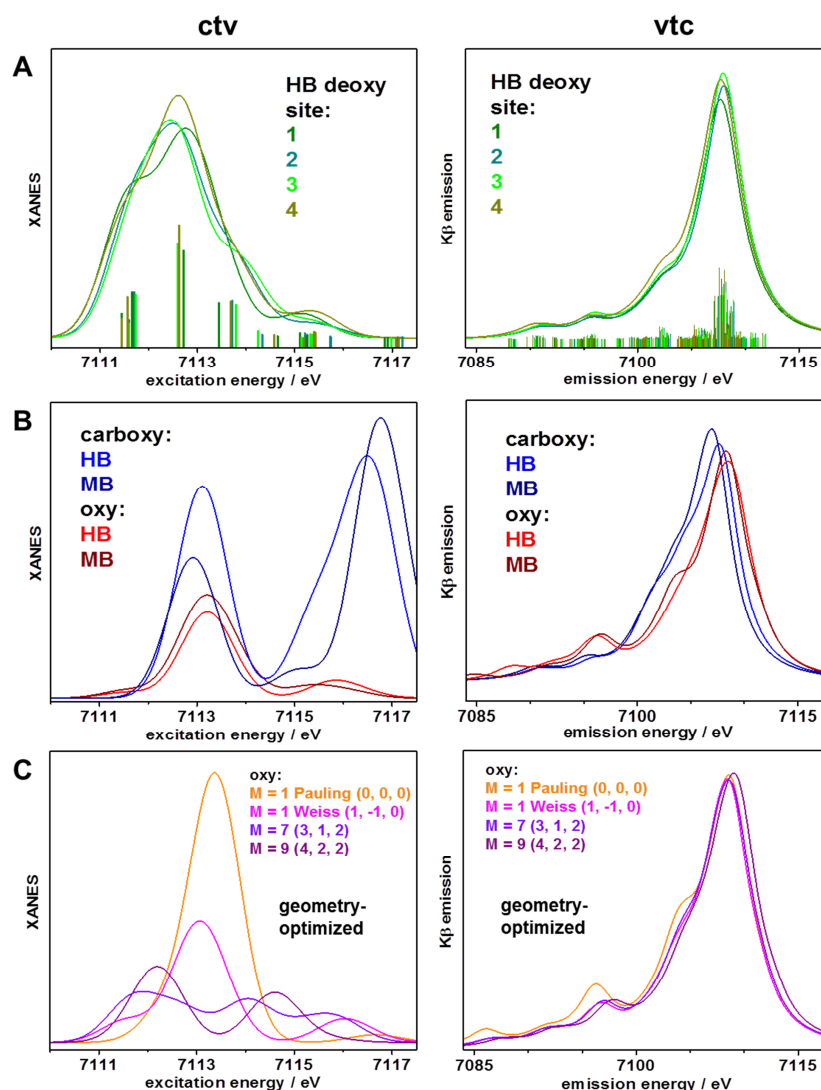


Figure S17: Heme ctv/vtc spectra for structure variation from (TD)DFT. (A) Calculated ctv and vtc spectra from single-point TDDFT or DFT on structures corresponding to the four **deoxy** heme sites in a HB crystal structure (PDB entry 2DN2, 1.25 Å resolution). (B) Calculated ctv/vtc spectra (single point) for **carboxy** or **oxy** heme sites in MB or HB (data for 4 heme sites in HB structure 2DN3, 1.25 Å resolution, and for 2 heme sites in MB structure 1A6G, 1.15 Å resolution, were averaged; LS Fe(II) in **carboxy** or LS Fe(III) in **oxy** (Weiss model) were assumed in the calculations). (C) Calculated ctv/vtc spectra for relaxed **oxy** heme structures based on HB crystal structure 2DN1 (1.25 Å resolution) and assuming (for $M = 1$) the Pauling model (LS Fe(II), afc-coupled spins on O_2) or the Weiss model (LS Fe(III), afc-coupling of spins on iron and O_2) in the calculations, or for assumed higher spin states (net spin on iron, O_2 , heme in parenthesis in the annotations). Note that the vtc spectra are quite insensitive to a spin state change and the ctv spectra show systematic peak amplitude/energy shifts for increasing unpaired spins on iron in **oxy**, so that the mean ctv/vtc spectra from data in C may be considered as an approximation for an IS Fe(II) species in **oxy** (Fig. 5).

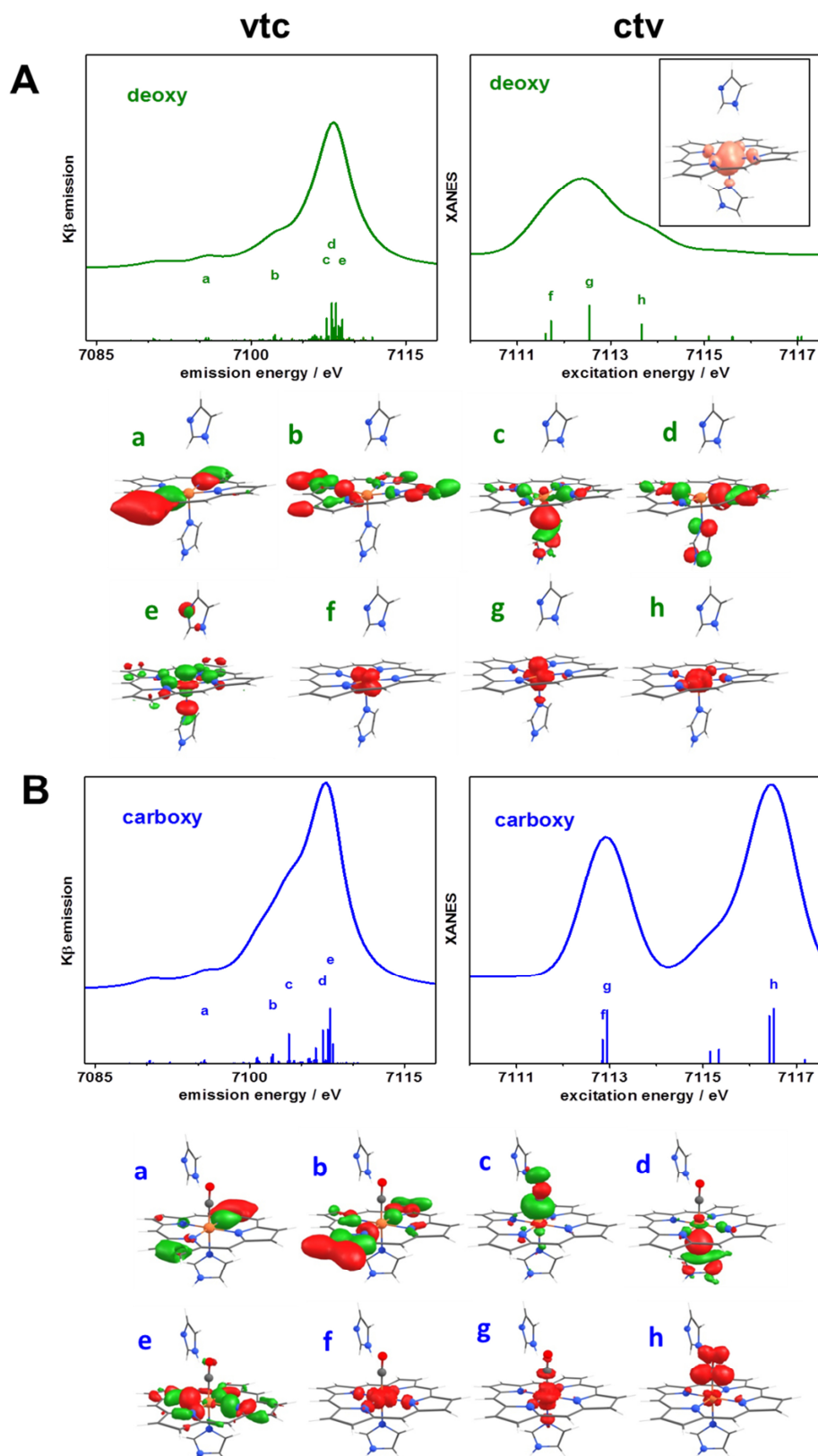


Figure S18A,B: Calculated ctv/vtc spectra of heme species and target/source MOs. Data from TDDFT (ctv) or DFT (vtc) correspond to geometry-optimized heme structures. (A) Data for **deoxy** (spin density distribution shown in the right inset). (B) Data for **carboxy**. MOs in the lower panels correspond to transitions (sticks) labeled a-h in the upper panels.

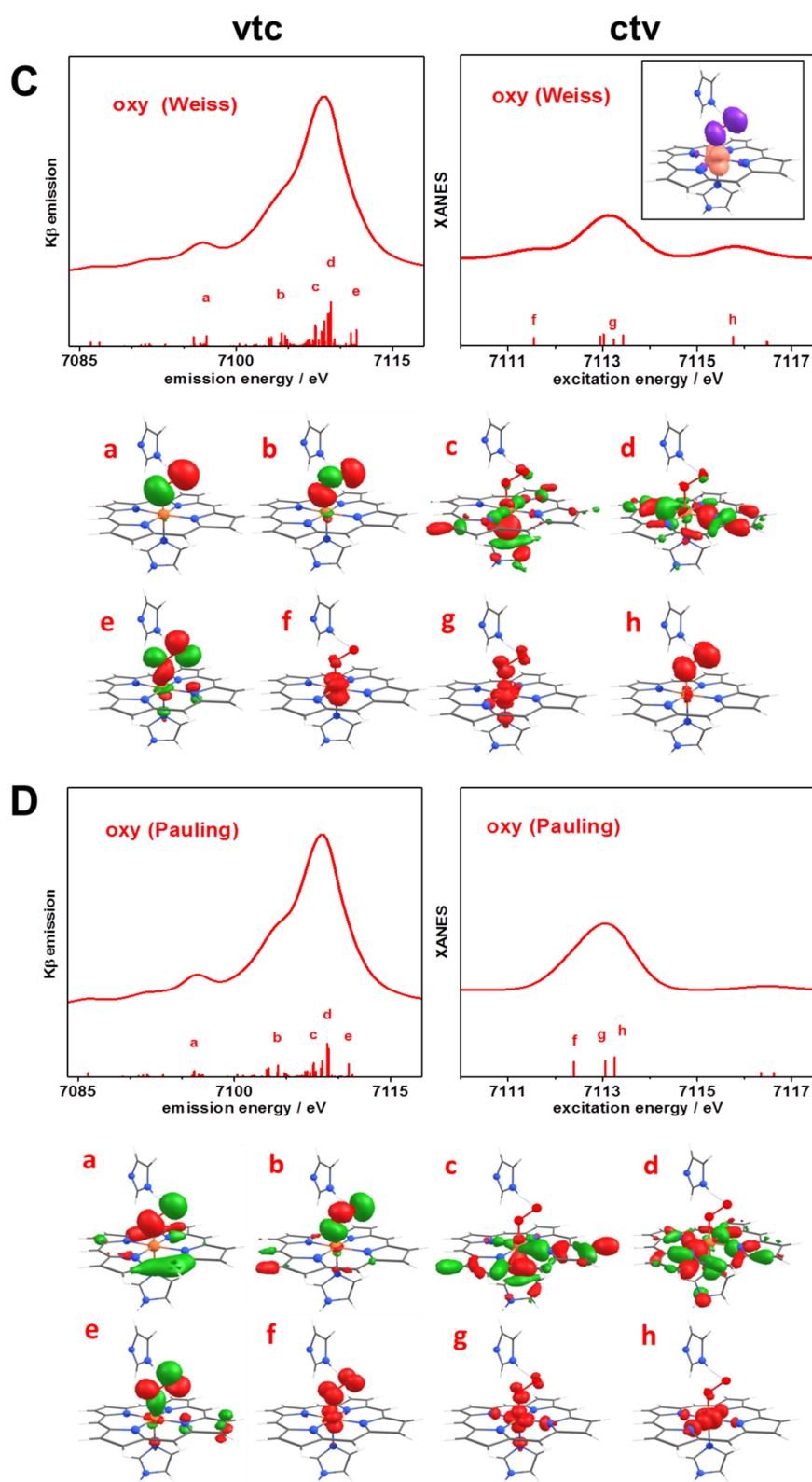


Figure S18C,D: Calculated ctv/vtc spectra of heme species and target/source MOs. Data from TDDFT (ctv) or DFT (vtc) correspond to geometry-optimized heme structures. (C) Data for the Weiss model of **oxy** (the spin density is shown in the right inset) (D) Data for the Pauling model of **oxy**. Shown MOs in the lower panels correspond to transitions (sticks) labeled a-h in the upper panels.

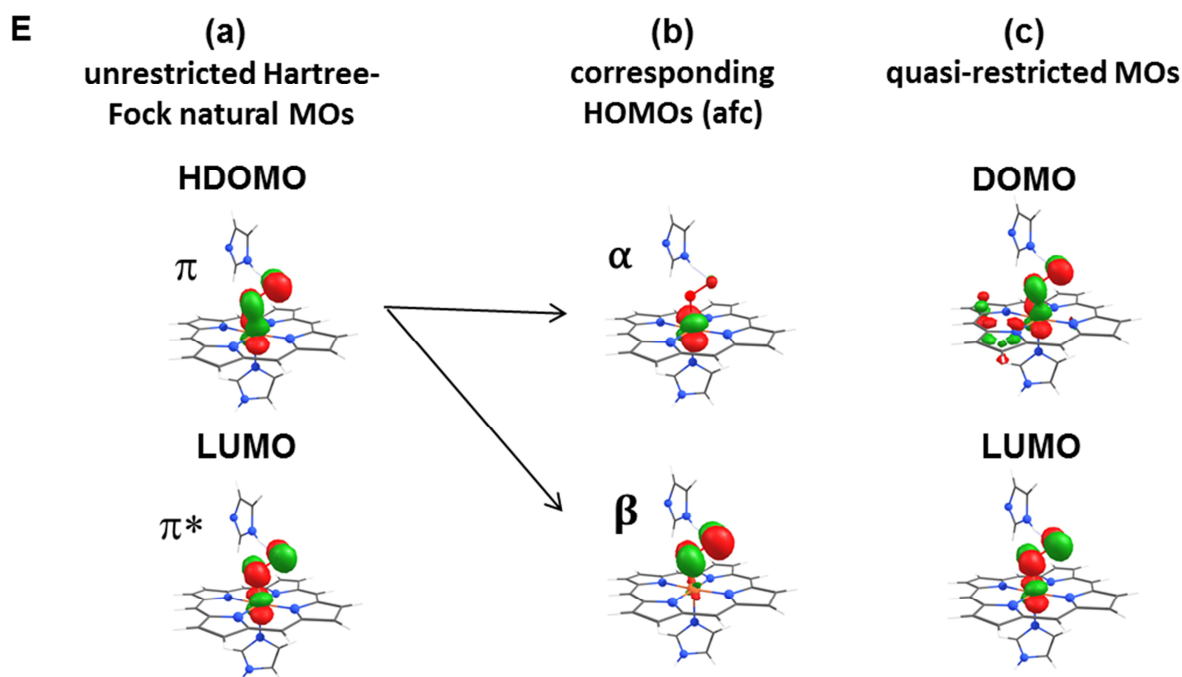


Figure S18E: Calculated ctv/vtc spectra of heme species and target/source MOs. (E) For geometry optimization of **oxy**, the DFT wavefunction for afc coupling converged, due to its single determinant nature, to a state similar to the Weiss model with a doublet O_2 and little charge transfer from iron to O_2 . This solution includes a double-occupied π Fe-O bonding MO at highest energy (HDOMO) and an unoccupied π^* Fe-O anti-bonding MO (LUMO) in the unrestricted Hartree-Fock natural MO representation (a). TDDFT predicts the lowest excitation into the Fe(d_{yz}) dominated MO and the highest transition into the $O_2(\pi^*_y)$ dominated MO, which are constructed from the unoccupied π^* Fe-O anti-bonding MO corresponding to the LUMO. The multi-configurational wavefunction from CASSCF includes partial occupancy of both the π^* Fe-O anti-bonding MO and the π Fe-O bonding MO. Therefore two additional ctv excitations into the Fe(d_{yz}) and $O_2(\pi_y)$ MOs stemming from the π Fe-O MO would be expected, which should be similar to the corresponding α/β HOMOs from DFT. The energy difference between the π (DOMO) and π^* (LUMO) Fe-O MOs from quasi-restricted DFT (c) is ~ 0.7 eV which would correspond to two excitations (into the Fe(d_{yz}) MOs) at lowest energies and two excitations (into the $O_2(\pi_y)$ and $O_2(\pi^*_y)$ MOs) at highest energies, in contrast to each one excitation according to the TDDFT solution. The CASSCF solution accordingly predicts that in effect the respective ctv spectrum shows three main features (at low, medium, and high energies), similar to the ctv spectrum from TDDFT for the Weiss model, but differing from the ctv spectrum for the Pauling model (Fig. S18C,D), and similar to the features observed in the experimental ctv spectrum of **oxy** (Fig. 4).

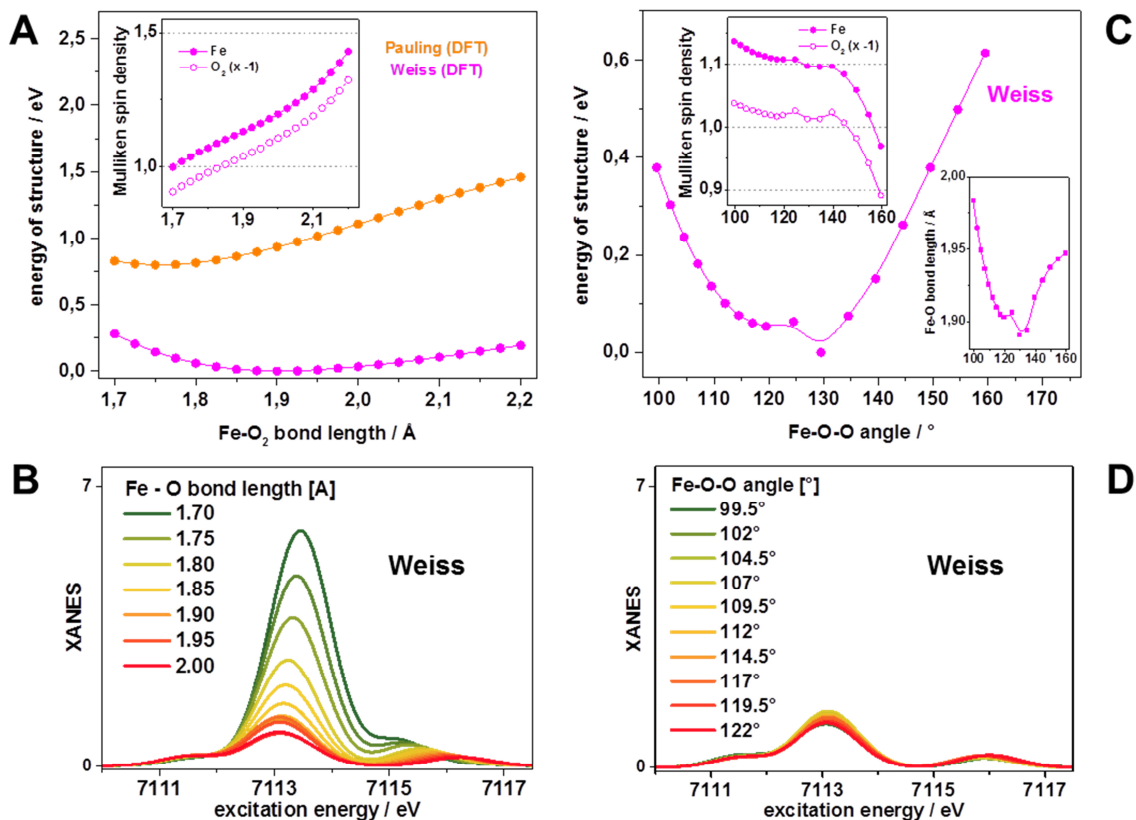


Figure S19: DFT energies and electron densities for **oxy** for Fe-O₂ bond geometry variation. Data refer to geometry-optimized structures from DFT with restraint Fe-O bond length or Fe-O-O angle. (A) Structure energies vs. Fe-O₂ bond length for Pauling (non-afc) or Weiss (afc) solutions (data shifted so that the Weiss minimum was set to zero energy) and Mulliken spin density on Fe and O₂ (x -1) in the inset. (B) ctv spectra from TDDFT for structures in (A). (C) Structure energies vs. Fe-O-O bond angle for the Weiss model (set to zero at the minimum), spin density on Fe and O₂ (x -1) in the top inset, and Fe-O bond length vs. Fe-O-O bond angle in the bottom inset (apparent discontinuities in energies and spin densities result from O₂ rotation vs. the heme principal axes). (D) ctv spectra from TDDFT for structures in (C). Note that the energy minimum for the Weiss model is ~0.75 eV lower vs. the Pauling model and that its Fe-O bond is ~0.15 Å longer (~1.9 Å), which is longer than the mean value from crystal structures and similar to the value from EXAFS for **oxy** in MB and HB (Table S2). The energy minimum for an angle of ~125 ° is similar to the mean (~127 ° from 10 structures), but rather variable angle (about 111-150 °) in crystal structures of **oxy**. The ctv spectrum is only moderately affected by small geometry changes around the energy minima. In the Weiss model the spin density on Fe and O₂ increases for increasing bond length and angle, apparently evolving in the directions of an O₂ triplet state and the CASSCF solution.

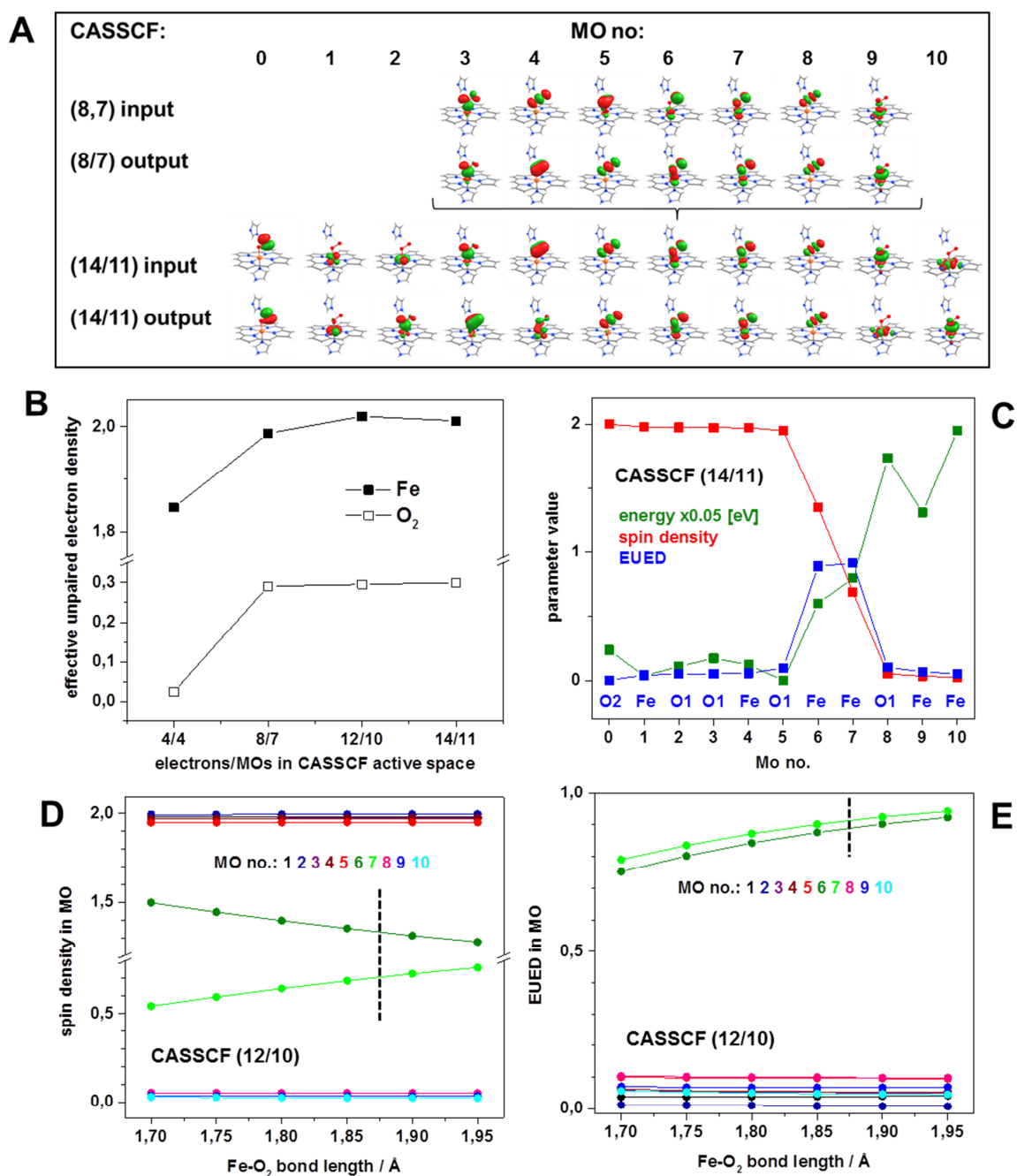


Figure S20: CASSCF data for active space and Fe-O₂ geometry variation. (A) Development of the MO configurations in a two-step CASSCF procedure (Fe-O₂ 1.875 Å). (B) Dependence of the total effective unpaired electron density (EUED) on active space size (Fe-O₂ 1.9 Å). (C) MO energy, spin density, and EUED for the largest active space (EUED attribution to atoms as indicated; Fe-O₂ 1.875 Å). (D) Spin density variation in MOs for Fe-O₂ bond length increase. (E) EUED variation in MOs for Fe-O₂ bond length increase. The energy minimum of structures in (D) and (E) is marked by vertical dashes; MO numbering as in A. Note that the EUED is calculated from the spin density (SD) in the natural molecular orbitals from CASSCF according to: $SD(MO) * [(2 - SD(MO))]$.

Chart S1: Coordinates of geometry-optimized heme and porphyrin structures.

(A) deoxy

55

Geometry optimized structure based on PDB entry 2DN2

Fe	-0.023974	0.007388	2.166448
N	2.074277	-0.017580	2.376724
N	-0.003382	-2.077587	2.502336
N	-2.037464	0.026650	2.742168
N	0.057888	2.103836	2.480259
C	2.871520	1.072390	2.485950
C	4.288200	0.657150	2.611190
C	4.208790	-0.771480	2.483330
C	2.905060	-1.134850	2.374950
C	2.357400	-2.456550	2.412020
C	1.113670	-2.961460	2.462140
C	0.668920	-4.206150	2.562160
C	-0.657710	-4.228980	2.554070
C	-1.156340	-2.851450	2.628550
C	-2.400970	-2.385790	2.725910
C	-2.882750	-1.076540	2.864670
C	-4.173580	-0.643300	3.195230
C	-4.066000	0.773840	3.227370
C	-2.815090	1.160550	2.960540
C	-2.381540	2.473550	2.950470
C	-1.089320	2.952610	2.712890
C	-0.517660	4.290860	2.644290
C	0.775720	4.290850	2.592370
C	1.235620	2.861640	2.411640
C	2.582480	2.412540	2.481570
N	-0.162633	0.011659	-0.018092
C	-0.239682	-1.087325	-0.851335
C	-0.264223	-0.672871	-2.152593
N	-0.200719	0.700626	-2.104004
C	-0.141430	1.073001	-0.807982
N	-0.045340	-2.011880	5.897550
C	-0.408010	-2.031420	7.241990
C	0.636570	-2.605710	7.879960
N	1.586970	-2.901930	6.922820
C	1.152820	-2.529340	5.735600
H	5.155207	1.289648	2.714261
H	5.044702	-1.456874	2.520346
H	3.140702	-3.215132	2.408914
H	1.299093	-5.087280	2.567309
H	-1.285729	-5.108682	2.611565
H	-3.173179	-3.148934	2.800056
H	-5.050124	-1.247069	3.370971
H	-4.886555	1.442508	3.454653
H	-3.136550	3.230194	3.136357
H	-1.130277	5.178628	2.759901

H	1.434378	5.147989	2.586871
H	3.373882	3.144625	2.545689
H	-0.271588	-2.089704	-0.460047
H	-0.319860	-1.211650	-3.082358
H	-0.198932	1.325220	-2.897285
H	-0.082393	2.099255	-0.486774
H	-0.619789	-1.632466	5.156840
H	-1.358208	-1.642842	7.567535
H	0.784536	-2.829529	8.923284
H	1.679037	-2.610417	4.803602

(B) carboxy

57

Geometry optimized structure based on PDB entry 2DN3

Fe	0.031233	-0.015408	2.043798
N	2.073297	-0.001448	1.989292
N	0.062843	-2.034437	2.055467
N	-2.001725	-0.057350	2.088411
N	-0.015143	2.002918	1.955952
C	2.906300	1.105780	2.081760
C	4.212970	0.717870	2.161070
C	4.246150	-0.690510	2.000220
C	2.895060	-1.104620	1.965080
C	2.495740	-2.378530	1.937750
C	1.183480	-2.819630	1.971020
C	0.822630	-4.265090	2.194220
C	-0.550300	-4.245800	2.344000
C	-1.027940	-2.847220	2.267410
C	-2.315800	-2.492510	2.373500
C	-2.792160	-1.139670	2.307750
C	-4.167240	-0.698320	2.497880
C	-4.157220	0.612290	2.310300
C	-2.850200	1.042350	2.111570
C	-2.467160	2.326820	2.036260
C	-1.100280	2.791620	1.949300
C	-0.744470	4.217760	1.988230
C	0.650500	4.211300	2.016120
C	1.069030	2.842250	2.024840
C	2.349220	2.410780	2.128740
N	-0.007196	-0.095146	-0.034844
C	-0.925343	-0.761515	-0.820806
C	-0.580295	-0.627225	-2.135450
N	0.568427	0.130563	-2.140235
C	0.879067	0.431339	-0.861477
N	2.364110	-2.046020	5.243840
C	2.142710	-1.722340	6.558230
C	3.143950	-2.314100	7.271640
N	3.961500	-2.954740	6.381770
C	3.474590	-2.784460	5.174760

H	5.066335	1.375912	2.242110
H	5.113796	-1.332643	1.991830
H	3.256918	-3.148988	1.898609
H	1.508972	-5.096978	2.195583
H	-1.204021	-5.089624	2.516593
H	-3.053595	-3.263653	2.555407
H	-5.005579	-1.351109	2.690835
H	-5.006188	1.281146	2.362401
H	-3.230588	3.094809	2.064426
H	-1.431608	5.048934	1.980112
H	1.318952	5.059094	2.053699
H	3.091421	3.200771	2.217094
H	-1.761223	-1.285675	-0.392379
H	-1.031478	-0.994878	-3.040519
H	1.088464	0.422399	-2.954490
H	1.737914	1.016237	-0.583367
H	1.799181	-1.766210	4.457307
H	1.297065	-1.126909	6.856383
H	3.333301	-2.304340	8.332512
H	3.888183	-3.171665	4.260600
C	-0.003275	0.089862	3.827681
O	-0.076848	0.172346	4.968614

(C) oxy

57

Geometry optimized structure based on PDB entry 2DN1

Fe	-0.018422	0.020345	2.060559
N	2.044100	0.034518	2.085061
N	-0.007896	-1.997196	2.130298
N	-2.046801	-0.043143	2.163759
N	0.017435	2.045239	1.993704
C	2.863280	1.191250	2.142050
C	4.172480	0.734780	2.104270
C	4.276140	-0.644720	2.011840
C	2.876020	-1.079090	1.996610
C	2.479730	-2.371740	1.949900
C	1.054650	-2.783290	2.087850
C	0.753510	-4.202130	2.343920
C	-0.530260	-4.197660	2.449280
C	-1.054180	-2.871440	2.311110
C	-2.334420	-2.443100	2.379670
C	-2.849660	-1.172220	2.355020
C	-4.173060	-0.792700	2.465200
C	-4.265960	0.671440	2.293840
C	-2.865960	1.044660	2.176780
C	-2.493760	2.410890	2.043570
C	-1.071020	2.838690	1.985570
C	-0.732830	4.256300	2.061980
C	0.636440	4.235780	2.153810

C	1.118750	2.882680	2.079990
C	2.380950	2.428130	2.092770
N	-0.031151	-0.077350	0.033811
C	-0.899128	-0.806536	-0.753405
C	-0.532934	-0.672534	-2.059158
N	0.572694	0.144928	-2.054323
C	0.843272	0.485997	-0.784897
N	1.442351	-1.597798	5.679640
C	1.454600	-1.620531	7.064540
C	2.617090	-2.192830	7.443740
N	3.315310	-2.497840	6.289910
C	2.575149	-2.132301	5.272600
H	5.022157	1.406840	2.136983
H	5.156257	-1.263700	1.965911
H	3.211809	-3.164140	1.892431
H	1.474508	-5.000841	2.388824
H	-1.181278	-5.043915	2.631757
H	-3.076020	-3.226489	2.516822
H	-5.003513	-1.469683	2.602950
H	-5.129495	1.313377	2.327786
H	-3.254939	3.175909	2.038565
H	-1.419608	5.085436	2.082232
H	1.294316	5.090153	2.238110
H	3.139513	3.208515	2.126117
H	-1.714069	-1.367659	-0.333872
H	-0.946499	-1.077290	-2.965772
H	1.090460	0.451365	-2.863704
H	1.662928	1.121750	-0.501912
H	0.681409	-1.233707	5.129738
H	0.622876	-1.232688	7.629181
H	3.003610	-2.394090	8.428920
H	2.847602	-2.246199	4.240944
O	-0.014237	0.246700	3.941009
O	-0.912770	-0.362852	4.662568

(D) Porphyrin compound 1

135

Fe(II) LS

Fe	0.000000	0.000000	0.000000
N	1.403045	1.312817	-0.580274
N	0.638636	0.192509	1.892915
N	-1.403045	-1.312817	0.580274
N	-0.638636	-0.192509	-1.892915
C	2.341130	1.969542	0.209454
C	2.487087	1.833910	1.599386
C	1.672500	0.990459	2.371768
C	1.804578	0.837522	3.803774
C	0.849925	-0.054571	4.196662
C	0.127576	-0.453367	3.008725

C	-0.934082	-1.367733	3.020790
C	-1.637316	-1.756734	1.872947
C	-2.732882	-2.700933	1.890636
C	-3.168449	-2.832534	0.604337
C	-2.341130	-1.969542	-0.209454
C	-2.487087	-1.833910	-1.599386
C	-1.672500	-0.990459	-2.371768
C	-1.804578	-0.837522	-3.803774
C	-0.849925	0.054571	-4.196662
C	-0.127576	0.453367	-3.008725
C	0.934082	1.367733	-3.020790
C	1.637316	1.756734	-1.872947
C	2.732882	2.700933	-1.890636
C	3.168449	2.832534	-0.604337
H	2.539634	1.354749	4.415074
H	0.640047	-0.420607	5.198371
H	-3.109222	-3.192564	2.783989
H	-3.975363	-3.453402	0.223566
H	-2.539634	-1.354749	-4.415074
H	-0.640047	0.420607	-5.198371
H	3.109222	3.192564	-2.783989
H	3.975363	3.453402	-0.223566
C	3.564151	2.627242	2.292453
C	3.290636	3.924931	2.785766
C	4.308813	4.647509	3.425339
C	5.596718	4.124502	3.595713
C	5.850237	2.840454	3.097336
C	4.861008	2.083982	2.451707
C	1.922751	4.548455	2.633494
C	6.667975	4.906788	4.319297
C	5.201432	0.705472	1.935115
H	4.085396	5.651755	3.799417
H	6.850524	2.410396	3.210736
H	1.149662	3.941114	3.130643
H	1.638837	4.636052	1.572668
H	1.901236	5.554583	3.075828
H	6.524217	5.990875	4.200460
H	7.671936	4.651923	3.948884
H	6.653982	4.691396	5.401138
H	6.250609	0.456792	2.149086
H	4.566590	-0.064202	2.402293
H	5.050272	0.638222	0.845943
C	-1.340549	-1.966628	4.339277
C	-2.323014	-1.331736	5.134095
C	-2.683784	-1.905912	6.362223
C	-2.101211	-3.092608	6.826464
C	-1.127581	-3.702746	6.024770
C	-0.736703	-3.163307	4.790091
C	-2.980844	-0.048713	4.681169
C	-2.531386	-3.711228	8.136590
C	0.320564	-3.860531	3.965387

H	-3.442180	-1.406812	6.974039
H	-0.653174	-4.627386	6.369080
H	-3.497673	-0.180909	3.717816
H	-2.239914	0.752636	4.534270
H	-3.716965	0.295627	5.421458
H	-2.857687	-2.945121	8.855542
H	-1.714819	-4.286903	8.597023
H	-3.377658	-4.403671	7.990070
H	0.667519	-4.775111	4.467014
H	-0.063810	-4.137784	2.971442
H	1.192339	-3.209265	3.796044
C	-3.564151	-2.627242	-2.292453
C	-4.861008	-2.083982	-2.451707
C	-5.850237	-2.840454	-3.097336
C	-5.596718	-4.124502	-3.595713
C	-4.308813	-4.647509	-3.425339
C	-3.290636	-3.924931	-2.785766
C	-5.201432	-0.705472	-1.935115
C	-6.667975	-4.906788	-4.319297
C	-1.922751	-4.548455	-2.633494
H	-6.850524	-2.410396	-3.210736
H	-4.085396	-5.651755	-3.799417
H	-4.566590	0.064202	-2.402293
H	-5.050272	-0.638222	-0.845943
H	-6.250609	-0.456792	-2.149086
H	-7.671936	-4.651923	-3.948884
H	-6.653982	-4.691396	-5.401138
H	-6.524217	-5.990875	-4.200460
H	-1.901236	-5.554583	-3.075828
H	-1.149662	-3.941114	-3.130643
H	-1.638837	-4.636052	-1.572668
C	1.340549	1.966628	-4.339277
C	0.736703	3.163307	-4.790091
C	1.127581	3.702746	-6.024770
C	2.101211	3.092608	-6.826464
C	2.683784	1.905912	-6.362223
C	2.323014	1.331736	-5.134095
C	-0.320564	3.860531	-3.965387
C	2.531386	3.711228	-8.136590
C	2.980844	0.048713	-4.681169
H	0.653174	4.627386	-6.369080
H	3.442180	1.406812	-6.974039
H	0.063810	4.137784	-2.971442
H	-1.192339	3.209265	-3.796044
H	-0.667519	4.775111	-4.467014
H	1.714819	4.286903	-8.597023
H	2.857687	2.945121	-8.855542
H	3.377658	4.403671	-7.990070
H	3.716965	-0.295627	-5.421458
H	3.497673	0.180909	-3.717816
H	2.239914	-0.752636	-4.534270

N	-1.298736	1.512947	0.284734
C	-2.581015	1.434137	-0.148354
C	-3.507676	2.459229	0.032338
C	-3.118677	3.630277	0.686668
C	-1.798832	3.718753	1.135019
C	-0.927852	2.652592	0.918510
H	-2.857639	0.513024	-0.654330
H	-4.524038	2.327750	-0.342074
H	-3.823114	4.449662	0.842421
H	-1.432394	4.606511	1.652779
H	0.103871	2.695684	1.257152
N	1.298736	-1.512947	-0.284734
C	2.581015	-1.434137	0.148354
C	3.507676	-2.459229	-0.032338
C	3.118677	-3.630277	-0.686668
C	1.798832	-3.718753	-1.135019
C	0.927852	-2.652592	-0.918510
H	2.857639	-0.513024	0.654330
H	4.524038	-2.327750	0.342074
H	3.823114	-4.449662	-0.842421
H	1.432394	-4.606511	-1.652779
H	-0.103871	-2.695684	-1.257152

(E) Porphyrin compound 2

139

Fe(II) HS

Fe	-0.000033	-0.001720	0.000223
N	-1.524319	-1.407731	0.002035
N	1.418071	-1.514917	0.001120
N	1.524275	1.404579	-0.001842
N	-1.417913	1.511774	-0.000941
C	-1.362317	-2.780139	0.003546
C	-0.127109	-3.468557	0.003978
C	1.156029	-2.870948	0.002967
C	2.410059	-3.597216	0.004118
C	3.418654	-2.668558	0.003159
C	2.792386	-1.360626	0.001396
C	3.489722	-0.128221	0.000037
C	2.884940	1.150698	-0.001663
C	3.605028	2.410702	-0.003217
C	2.667311	3.409846	-0.004485
C	1.362359	2.777069	-0.003544
C	0.127178	3.465527	-0.003999
C	-1.155941	2.867873	-0.002796
C	-2.409994	3.594053	-0.003713
C	-3.418568	2.665337	-0.002593
C	-2.792323	1.357433	-0.000989
C	-3.489652	0.125040	0.000329
C	-2.884871	-1.153879	0.001868

C	-3.604999	-2.413902	0.003239
C	-2.667267	-3.413008	0.004349
H	2.504086	-4.680699	0.005609
H	4.490908	-2.848259	0.003651
H	4.687670	2.511157	-0.003396
H	2.840186	4.483561	-0.005850
H	-2.504091	4.677532	-0.005163
H	-4.490826	2.845018	-0.002907
H	-4.687638	-2.514386	0.003387
H	-2.840086	-4.486732	0.005546
C	-0.181558	-4.973235	0.006129
C	-0.203872	-5.684756	-1.215910
C	-0.250919	-7.086617	-1.191013
C	-0.278267	-7.807076	0.010257
C	-0.251500	-7.083083	1.209401
C	-0.204469	-5.681146	1.230252
C	-0.174051	-4.957706	-2.540685
C	-0.364195	-9.315908	0.012419
C	-0.175184	-4.950192	2.552879
H	-0.264002	-7.629922	-2.141389
H	-0.265030	-7.623602	2.161350
H	0.732347	-4.339872	-2.638339
H	-1.034290	-4.277746	-2.643036
H	-0.197052	-5.669624	-3.378017
H	0.118200	-9.747751	-0.876964
H	-1.414337	-9.653942	0.011530
H	0.115859	-9.745056	0.904358
H	-0.198007	-5.659667	3.392282
H	0.730882	-4.331631	2.648870
H	-1.035654	-4.270246	2.653172
C	4.996423	-0.185073	0.000511
C	5.710547	-0.210216	-1.220849
C	7.112291	-0.262218	-1.197961
C	7.835134	-0.292180	0.001236
C	7.111658	-0.262884	1.200037
C	5.709879	-0.210785	1.222233
C	4.990468	-0.175034	-2.548396
C	9.343422	-0.384592	0.001607
C	4.989299	-0.175388	2.549519
H	7.653383	-0.278362	-2.149519
H	7.652244	-0.279554	2.151876
H	4.416858	0.757881	-2.667015
H	4.274133	-1.006233	-2.637734
H	5.703739	-0.244621	-3.381941
H	9.776307	0.096604	-0.887900
H	9.676731	-1.436226	-0.000498
H	9.775604	0.092858	0.893462
H	5.701894	-0.249895	3.383225
H	4.420141	0.760072	2.669912
H	4.269031	-1.003353	2.636864
C	0.181609	4.970212	-0.006490

C	0.204447	5.677841	-1.230781
C	0.251402	7.079790	-1.210320
C	0.278185	7.804111	-0.011374
C	0.250941	7.083953	1.190076
C	0.203956	5.682104	1.215327
C	0.175302	4.946588	-2.553248
C	0.364014	9.312946	-0.013943
C	0.174204	4.955446	2.540315
H	0.264849	7.620055	-2.162419
H	0.264054	7.627506	2.140307
H	-0.730139	4.327023	-2.648669
H	1.036537	4.267617	-2.653786
H	0.196971	5.655911	-3.392813
H	1.414137	9.651043	-0.013181
H	-0.116097	9.741822	-0.905983
H	-0.118378	9.744996	0.875339
H	0.197660	5.667578	3.377449
H	-0.732429	4.338003	2.638351
H	1.034265	4.275245	2.642606
C	-4.996361	0.181816	-0.000021
C	-5.709918	0.207641	-1.221680
C	-7.111699	0.259474	-1.199374
C	-7.835098	0.288383	-0.000514
C	-7.112163	0.258285	1.198622
C	-5.710403	0.206535	1.221393
C	-4.989396	0.172702	-2.548998
C	-9.343405	0.380451	-0.000761
C	-4.990217	0.171318	2.548879
H	-7.652360	0.276174	-2.151169
H	-7.653188	0.274059	2.150226
H	-4.418558	-0.761781	-2.668890
H	-4.270611	1.001912	-2.636827
H	-5.702167	0.245540	-3.382698
H	-9.676957	1.432008	0.001148
H	-9.776092	-0.100656	0.888890
H	-9.775566	-0.097287	-0.892472
H	-5.703589	0.238583	3.382528
H	-4.414615	-0.760489	2.666444
H	-4.275618	1.003940	2.639081
O	-0.000337	-0.004447	-2.316105
C	-1.192463	-0.012727	-3.149860
C	-0.703763	-0.343984	-4.561435
C	0.701082	0.285677	-4.570810
C	1.191993	-0.004181	-3.150399
H	-1.659617	0.985880	-3.100020
H	-1.888928	-0.750591	-2.729832
H	-1.365936	0.061380	-5.339516
H	-0.636465	-1.434352	-4.700640
H	0.633231	1.371442	-4.742174
H	1.362900	-0.141810	-5.337244
H	1.881121	0.751753	-2.750499

H	1.669152	-0.996072	-3.073500
O	0.000385	-0.001772	2.316254
C	1.192155	0.021517	3.150073
C	0.703221	0.384208	4.553629
C	-0.700759	-0.246895	4.576979
C	-1.192291	0.010034	3.150228
H	1.890283	0.748436	2.714194
H	1.657020	-0.979091	3.122484
H	0.634587	1.477407	4.667638
H	1.365756	-0.002491	5.340851
H	-1.363307	0.196862	5.333468
H	-0.631351	-1.328370	4.773088
H	-1.674015	0.997678	3.051325
H	-1.877888	-0.757708	2.766916

(F) Porphyrin compound 3

114

Fe(III) HS

Fe	-0.339367	0.414748	0.055270
N	0.617844	0.743323	-1.751554
N	1.425425	1.053670	0.928603
N	-0.627027	-0.730998	1.753179
N	-1.435253	-1.040936	-0.925819
C	1.664576	1.599857	-1.969669
C	2.484781	2.164397	-0.996506
C	2.360826	1.870862	0.361629
C	3.281078	2.359394	1.364644
C	2.899714	1.793687	2.528280
C	1.739999	0.995179	2.256298
C	1.047644	0.279787	3.232466
C	-0.066066	-0.490034	2.981805
C	-0.801947	-1.196208	3.997131
C	-1.783146	-1.876711	3.377773
C	-1.664576	-1.599857	1.969669
C	-2.484781	-2.164397	0.996506
C	-2.360826	-1.870862	-0.361629
C	-3.281078	-2.359394	-1.364644
C	-2.899714	-1.793687	-2.528280
C	-1.739999	-0.995178	-2.256298
C	-1.047643	-0.279787	-3.232465
C	0.066066	0.490033	-2.981805
C	0.801947	1.196208	-3.997131
C	1.783146	1.876711	-3.377773
H	4.110438	3.022118	1.182304
H	3.352739	1.910293	3.498897
H	-0.578704	-1.173381	5.051053
H	-2.522423	-2.522339	3.822113
H	-4.101959	-3.033382	-1.185062
H	-3.344900	-1.921758	-3.501148

H	0.587383	1.162094	-5.052573
H	2.531068	2.511336	-3.823510
C	3.562400	3.115757	-1.430728
C	3.315317	4.491881	-1.433225
C	4.317580	5.351153	-1.865774
C	5.546425	4.899551	-2.275045
C	5.783964	3.520818	-2.249830
C	4.806576	2.629045	-1.836707
C	1.995463	5.043503	-0.976409
C	6.618292	5.853605	-2.745629
C	5.102238	1.154857	-1.820648
H	4.113845	6.417462	-1.878327
H	6.749416	3.138235	-2.563480
H	1.879009	4.968198	0.108553
H	1.156754	4.503992	-1.419853
H	1.902574	6.094996	-1.251442
H	6.335905	6.888248	-2.546904
H	6.796751	5.748648	-3.819704
H	7.567604	5.657419	-2.241888
H	6.097717	0.953738	-2.217590
H	5.055414	0.747307	-0.807427
H	4.383504	0.591924	-2.419923
C	1.567406	0.345128	4.640668
C	1.146372	1.361194	5.495269
C	1.636800	1.388325	6.788980
C	2.517609	0.433509	7.271820
C	2.937755	-0.539379	6.409579
C	2.471382	-0.612910	5.099340
C	0.167330	2.406660	5.019153
C	2.999546	0.496526	8.701146
C	2.917500	-1.728346	4.209155
H	1.291577	2.172632	7.455330
H	3.629241	-1.302772	6.752953
H	-0.720941	1.952752	4.575377
H	0.613545	3.045468	4.252260
H	-0.153038	3.045826	5.842412
H	2.435673	1.236595	9.269830
H	4.056858	0.771787	8.755895
H	2.881006	-0.469264	9.198160
H	3.577053	-2.413681	4.742129
H	2.073790	-2.305592	3.823859
H	3.461326	-1.353502	3.337290
C	-3.562400	-3.115757	1.430728
C	-4.806576	-2.629045	1.836707
C	-5.783964	-3.520818	2.249830
C	-5.546425	-4.899551	2.275045
C	-4.317580	-5.351153	1.865774
C	-3.315317	-4.491881	1.433225
C	-5.102238	-1.154857	1.820648
C	-6.618292	-5.853605	2.745629
C	-1.995463	-5.043503	0.976409

H	-6.749278	-3.138132	2.563780
H	-4.113837	-6.417467	1.878523
H	-5.065530	-0.749782	0.806020
H	-4.377076	-0.589820	2.409616
H	-6.093869	-0.953237	2.226935
H	-6.797747	-5.747821	3.819449
H	-7.567262	-5.658224	2.240909
H	-6.335359	-6.888305	2.547949
H	-1.900080	-6.093532	1.256164
H	-1.882214	-4.974703	-0.109441
H	-1.156602	-4.501087	1.416187
C	-1.567406	-0.345128	-4.640668
C	-2.471382	0.612910	-5.099340
C	-2.937755	0.539379	-6.409579
C	-2.517609	-0.433509	-7.271820
C	-1.636800	-1.388325	-6.788980
C	-1.146372	-1.361194	-5.495269
C	-2.917500	1.728346	-4.209155
C	-2.999546	-0.496526	-8.701146
C	-0.167330	-2.406660	-5.019153
H	-3.629352	1.302722	-6.752817
H	-1.291442	-2.172474	-7.455458
H	-2.073832	2.311653	-3.833718
H	-3.448599	1.353716	-3.330052
H	-3.586318	2.406929	-4.739341
H	-4.056664	-0.772542	-8.755901
H	-2.435183	-1.236042	-9.270076
H	-2.881727	0.469496	-9.197872
H	0.166026	-3.035003	-5.845699
H	0.713709	-1.953837	-4.560066
H	-0.619564	-3.057453	-4.265765
Cl	-1.824553	2.129254	0.223827

Chart S2: Example of input files for (TD)DFT and MP2/CASSCF.

```
#####  
# 1st Step (a): Rough optimization of Fe - O - O, axial histidine and porphyrin #  
# nitrogen constraining the distal histidine and carbon atoms on porphyrin #  
#####  
'2DN1_AN2175_a_BP86.inp'  
!UKS BP86 TZVP TZVP/J RIJCOSX tightopt cosmo(water) PAL8  
%maxcore 1000  
%method Z_GridX 2 end  
%geom  
  Constraints  
  {B 0 55 1.70 C}  
  {C 5 C}  
  {C 6 C}  
  {C 7 C}  
  {C 8 C}  
  {C 9 C}  
  {C 10 C}  
  {C 11 C}  
  {C 12 C}  
  {C 13 C}  
  {C 14 C}  
  {C 15 C}  
  {C 16 C}  
  {C 17 C}  
  {C 18 C}  
  {C 19 C}  
  {C 20 C}  
  {C 21 C}  
  {C 22 C}  
  {C 23 C}  
  {C 24 C}  
  {C 30 C}  
  {C 31 C}  
  {C 32 C}  
  {C 33 C}  
  {C 34 C}  
end  
end  
%scf  
  DirectResetFreq 10  
  TCut 1e-14  
  Thresh 1e-12  
  MaxCore 2000  
  MaxIntMem 2000  
  maxiter 5000  
  Damp fac 0.8 ErrOff 0.0005 Min 0.0 Max 0.8 end  
  CNVZerner true  
  Shift Shift 0.4 ErrOff 0.0 end
```

```
DIIS Start 0.01 end
BrokenSym 2,2
end
* xyzfile 0 5 2DN1_AN2175.xyz
```

```
#####
# (1st Step (b): Potential energy surface scan from 1.7A to 2.2A with B3LYP) #
#####
'2DN1_AN2175_b_geom-scan.inp'
!UKS B3LYP TZVP TZVP/J RIJCOSX tightopt cosmo(water) PAL8
%maxcore 1000
%method Z_GridX 2 end
%geom
  MaxIter 500
  scan B 0 55 = 1.7, 2.2, 21 end
  Constraints
    {C 5 C}
    {C 6 C}
    {C 7 C}
    {C 8 C}
    {C 9 C}
    {C 10 C}
    {C 11 C}
    {C 12 C}
    {C 13 C}
    {C 14 C}
    {C 15 C}
    {C 16 C}
    {C 17 C}
    {C 18 C}
    {C 19 C}
    {C 20 C}
    {C 21 C}
    {C 22 C}
    {C 23 C}
    {C 24 C}
    {C 30 C}
    {C 31 C}
    {C 32 C}
    {C 33 C}
    {C 34 C}
  end
end
%scf
  DirectResetFreq 10
  TCut 1e-14
  Thresh 1e-12
  MaxCore 2000
  MaxIntMem 2000
  maxiter 5000
```

```

    Damp fac 0.8 ErrOff 0.0005 Min 0.0 Max 0.8 end
    CNVZerner true
    Shift Shift 0.4 ErrOff 0.0 end
    DIIS Start 0.01 end
    BrokenSym 2,2
end
* xyzfile 0 5 2DN1_AN2175_a_BP86.xyz

#####
# 2nd Step: Calculation of v2c and c2v spectra      #
#####
'2DN1_AN2175_c_geom-scan-spec.009.inp'
!UKS B3LYP def2-TZVP def2-TZVP/J RIJCOSX
!tightscf moread
!Grid4 FinalGrid5 cosmo(water)
!PAL8 UCO
%maxcore 1000
%method Z_GridX 2 end
%output Print[P_ReducedOrbPopMO_M] = 1 end
%moinp "2DN1_AN2175_b_geom-scan.009.gbw"
%scf
    DirectResetFreq 10
    TCut 1e-14
    Thresh 1e-12
    MaxCore 2000
    MaxIntMem 2000
    maxiter 5000
    Damp fac 0.8 ErrOff 0.0005 Min 0.0 Max 0.8 end
    CNVZerner true
    Shift Shift 0.4 ErrOff 0.0 end
    DIIS Start 0.01 end
end
%xes
    DoQuad true # Switch for the calculation of magnetic dipole and electric quadrupole
transition moments
    DoXAS true # Do absorbtion
    CoreOrb 0,0 # List of core orbitals in which a hole is generated
    OrbOp 0,1 # The operators for each CoreOrb (0: spin up, 1: spin down)
    Normalize false # if set to true, most intensive feature will be set to 1 (default true)
end
%tddft
    orbwin[0] = 0,0,-1,-1
    orbwin[1] = 0,0,-1,-1
    doquad true
    nroots 20
    maxdim 200
end
* xyzfile 0 1 2DN1_AN2175_b_geom-scan.009.xyz

```

```

#####
# 3rd Step: Using geometries from 2nd step for final optimization on final #
#      basis set                                #
#####
'2DN1_AN2175-afc_1.90A_a_opt.inp'
!UKS B3LYP def2-TZVP def2-TZVP/JK RIJCOSX
!tightopt moread
!Grid4 GridX4 NoFinalGrid cosmo(water)
!PAL8 UNO UCO
%maxcore 1000
%method Z_GridX 3 end
%output Print[P_ReducedOrbPopMO_M] = 1 end
%moinp "2DN1_AN2175_c_geom-scan-spec.009.gbw"
%geom
    MaxIter 500
    Constraints
    {B 0 55 1.90 C}
    {C 5 C}
    {C 6 C}
    {C 7 C}
    {C 8 C}
    {C 9 C}
    {C 10 C}
    {C 11 C}
    {C 12 C}
    {C 13 C}
    {C 14 C}
    {C 15 C}
    {C 16 C}
    {C 17 C}
    {C 18 C}
    {C 19 C}
    {C 20 C}
    {C 21 C}
    {C 22 C}
    {C 23 C}
    {C 24 C}
    {C 30 C}
    {C 31 C}
    {C 32 C}
    {C 33 C}
    {C 34 C}
end
end
%scf
    DirectResetFreq 10
    TCut 1e-14
    Thresh 1e-12
    MaxCore 2000
    MaxIntMem 2000
    maxiter 5000

```

```

    Damp fac 0.8 ErrOff 0.0005 Min 0.0 Max 0.8 end
    CNVZerner true
    Shift Shift 0.4 ErrOff 0.0 end
    DIIS Start 0.01 end
end
* xyzfile 0 1 2DN1_AN2175_c_geom-scan-spec.009.xyz

#####
# 4th Step: Using geometries from 3rd step for an MP2 calculation with RI      #
#      approximation and unrelaxed density                                  #
#####
'2DN1_AN2175-afc_1.90A_b_RIMP2.inp'
!UKS RI-MP2 def2-TZVP def2-TZVP/JK RIJCOSX
!tightscf moread
!Grid4 GridX4 FinalGrid5 cosmo(water)
!PAL8 UNO UCO
%maxcore 1000
%method Z_GridX 3 end
%output Print[P_ReducedOrbPopMO_M] = 1 end
%moinp "2DN1_AN2175-afc_1.90A_a_opt.gbw"
%MP2
    density unrelaxed
    natorbs true
end
%scf
    DirectResetFreq 10
    TCut 1e-14
    Thresh 1e-12
    MaxCore 2000
    MaxIntMem 2000
    maxiter 5000
    Damp fac 0.8 ErrOff 0.0005 Min 0.0 Max 0.8 end
    CNVZerner true
    Shift Shift 0.4 ErrOff 0.0 end
    DIIS Start 0.01 end
end
* xyzfile 0 1 2DN1_AN2175-afc_1.90A_a_opt.xyz

#####
# 5th Step: Performing CAS(8,7) with orbitals from separately localizing the  #
#      internal and external space of the MP2 natural orbitals              #
#####
'2DN1_AN2175-afc_1.90A_c_CAS8-7_n1.inp'
!def2-TZVP def2-TZVP/JK
!moread
!Grid4 GridX3 cosmo(water)
!LooseSCF PAL4
%maxcore 2500
%output

```

```

    localspin 0, 55, 56, 1, 2, 3, 4, 25
    Print[P_ReducedOrbPopMO_M] = 1
    print[p_unpaired_t] 1
    print[p_unpaired_hg] 1
end
%moinp "2DN1_AN2175-afc_1.90A_b_RIMP2_VMO.loc.mp2nat"
%scf
    rotate
        {139, 137, 90}

        {96, 136, 90}
        {95, 135, 90}
        {97, 134, 90}
        {94, 133, 90}
    end
end
%casscf
    nel 8
    norb 7
    mult 1
    nroots 1
    OrbStep DIIS
    SwitchStep SOSCF
    SwitchConv 0.03
    SwitchIter 25
    MaxIter 100
    FreezeIE 0.3
    FreezeActive 0.05
    trafostep rimo
    SwitchDens 0.000001
    ResetFreq 1
    shiftup 1.5
    shiftdn 1.5
    ci
        secshift 0.2
        NGuessMat 3096
    end
end
%method
    Z_GridX    3
end
* xyzfile 0 1 2DN1_AN2175-afc_1.90A_b_RIMP2.xyz

```

```

#####
# 6th Step: Performing CAS(12,10) with orbitals from separately localizing the #
#      internal and external space of the CAS(8,7) calculation          #
#####
'2DN1_AN2175-afc_1.90A_d_CAS12-10_n1.inp'
!def2-TZVP def2-TZVP/JK
!moread

```

```

!Grid4 GridX3 cosmo(water)
!LooseSCF PAL4
%maxcore 2500
%output
    localspin 0, 55, 56, 1, 2, 3, 4, 25
    Print[P_ReducedOrbPopMO_M] = 1
    print[p_unpaired_t] 1
    print[p_unpaired_hg] 1
end
%moinp "2DN1_AN2175-afc_1.90A_c_CAS8-7_n1_VMO.loc.gbvw"
%scf
    rotate
        {168, 140, 90}

        {87, 132, 90}
        {85, 131, 90}
    end
end
%casscf
    nel 12
    norb 10
    mult 1
    nroots 1
    OrbStep DIIS
    SwitchStep KDIIS
    SwitchConv 0.03
    SwitchIter 25
    MaxIter 100
    FreezeIE 0.3
    FreezeActive 0.05
    trafostep rimo
    SwitchDens 0.000001
    ResetFreq 1
    shiftup 1.5
    shiftdn 1.5
    ci
        secshift 0.2
        NGuessMat 3096
    end
end
%method
    Z_GridX    3
end
* xyzfile 0 1 2DN1_AN2175-afc_1.90A_b_RIMP2.xyz

```

```

#####
# 7th Step: Adding the remaining 2pz orbital on terminal oxygen for a CAS(14,11)#
#####
'2DN1_AN2175-afc_1.90A_e_CAS14-11_n1.inp'
!def2-TZVP def2-TZVP/JK RIJCOSX

```

```

!moread
!Grid4 GridX3 cosmo(water)
!LooseSCF
%maxcore 2500
%output
    localspin 0, 55, 56, 1, 2, 3, 4, 25
    Print[P_ReducedOrbPopMO_M] = 1
    print[p_unpaired_t] 1
    print[p_unpaired_hg] 1
end
%moinp "2DN1_AN2175-afc_1.90A_d_CAS12-10_n1_OMO.loc.gbw"
%scf
    rotate
        {102, 130, 90}
    end
end
%casscf
    nel 14
    norb 11
    mult 1
    nroots 1
    OrbStep DIIS
    SwitchStep KDIIS
    SwitchConv 0.03
    SwitchIter 25
    MaxIter 100
    FreezeIE 0.5
    FreezeActive 0.05
    trafostep rimo
    SwitchDens 0.000001
    ResetFreq 1
    shiftup 1.5
    shiftdn 1.5
    ci
        secshift 0.2
        NGuessMat 3096
    end
end
%method
    Z_GridX      3
end
* xyzfile 0 1 2DN1_AN2175-afc_1.90A_b_RIMP2.xyz

```


Supporting References

1. Mebs M, Braun N, Kositzki R, Limberg C, & Haumann M (2015) Abrupt versus gradual spin-crossover in Fe(II)(phen)₂(NCS)₂ and Fe(III)(dedtc)₃ compared by X-ray absorption and emission spectroscopy and quantum-chemical calculations. *Inorg Chem* 54:11606-11624.
2. Zaharieva I, *et al.* (2016) Room-temperature energy-sampling K β X-ray emission spectroscopy of the Mn₄Ca complex of photosynthesis reveals three manganese-centered oxidation steps and suggests a coordination change prior to O₂ formation. *Biochemistry* 55(30):4197-4211.
3. Kositzki R, *et al.* (2016) Protonation state of MnFe and FeFe cofactors in a ligand binding oxidase revealed by X ray absorption, emission, and vibrational spectroscopy and QM/MM calculations. *Inorg Chem* 19:9869-9885.
4. Yao S, *et al.* (2015) Biomimetic reduced [2Fe–2S] clusters with unprecedentedly delocalized mixed-valence iron centers. *Angew. Chem. Int. Ed. Engl.* 54:12506-12510.
5. Lambertz C, *et al.* (2014) Electronic and molecular structures of the [2Fe] and [4Fe4S] units of the active-site H-cluster in [FeFe]-hydrogenase determined by spin- and site-selective XAE and DFT. *Chem Sci* 5:1187-1203.
6. Huwald D, Schrapers P, Kositzki R, Haumann M, & Hemschemeier A (2015) Characterization of unusual truncated hemoglobins of *Chlamydomonas reinhardtii* suggests specialized functions. *Planta* 242:167-185.
7. Rehr JJ, Kas JJ, Vila FD, Prange MP, & Jorissen K (2010) Parameter-free calculations of X-ray spectra with FEFF9. *Phys Chem Chem Phys* 12(21):5503-5513.
8. Neese F (2012) The ORCA program system. *Wires Comput Mol Sci* 2(1):73-78.
9. Neese F (2008) ORCA: An ab-initio, DFT, and semiempirical electronic structure package. v.2.6.35. Theoretical Chemistry Group. (Max-Planck Institute for Chemical Energy Conversion, Mülheim, Germany).
10. Takatsuka K, Fueno T, & Yamaguchi K (1978) Distribution of odd Electrons in ground-state molecules. *Theor Chim Acta* 48(3):175-183.
11. Vankó G, *et al.* (2006) Probing the 3d spin momentum with X-ray emission spectroscopy: the case of molecular-spin transitions. *J. Phys. Chem. B* 110:11647-11653.
12. de Groot F (2001) High-resolution X-ray emission and X-ray absorption spectroscopy. *Chem Rev* 101(6):1779-1808.
13. Wang X, De Groot F, & Cramer SP (1997) Spin-polarized x-ray emission of 3d transition metal ions - a comparison via K α and K β detection. *Phys Rev B* 56:4553-4564.
14. Tsutsumi K, Nakamori H, & Ichikawa K (1976) X-ray Mn K β emission-spectra of manganese oxides and manganates. *Phys Rev B* 13(2):929-933.
15. Peng G, *et al.* (1994) High-resolution manganese X-ray-fluorescence spectroscopy - oxidation-state and spin-state sensitivity. *J Am Chem Soc* 116(7):2914-2920.

16. Pollock CJ, Delgado-Jaime MU, Atanasov M, Neese F, & DeBeer S (2014) K beta mainline X-ray emission spectroscopy as an experimental probe of metal-ligand covalency. *J Am Chem Soc* 136(26):9453-9463.
17. Glatzel P, Jacquamet L, Bergmann U, de Groot FMF, & Cramer SP (2002) Site-selective EXAFS in mixed-valence compounds using high-resolution fluorescence detection: A study of iron in Prussian Blue. *Inorg Chem* 41(12):3121-3127.
18. Glatzel P, Bergmann U, de Groot FMF, & Cramer SP (2001) Influence of the core hole on K beta emission following photoionization or orbital electron capture: A comparison using MnO and (Fe₂O₃)-Fe-55. *Phys Rev B* 64(4).
19. Hamalainen K, *et al.* (1992) Spin-dependent X-ray absorption of MnO and MnF₂. *Phys Rev B* 46(21):14274-14277.
20. Zaharieva I, *et al.* (2009) Towards a comprehensive X-ray approach for studying the photosynthetic manganese complex—XANES, K-alpha/K-beta/K-beta-satellite emission lines, RIXS, and comparative computational approaches for selected model complexes. *J Phys Conf Ser* 190:012142, 012141-012146.
21. Glatzel P & Bergmann U (2005) High resolution 1s core hole X-ray spectroscopy in 3d transition metal complexes - electronic and structural information. *Coord Chem Rev* 249(1-2):65-95.
22. Sakurai K, Eba H, Numako C, & Iihara J (2000) Trace chemical characterization using monochromatic X-ray undulator radiation. *Anal Chem* 72(11):2613-2617.
23. Degroot FMF, Fontaine A, Kao CC, & Krisch M (1994) Charge-transfer multiplet calculations of the K-beta X-ray-emission spectra of divalent nickel compounds. *J Phys Condens Matt* 6(34):6875-6884.
24. Leidel N, *et al.* (2013) Bridging-hydride influence on the electronic structure of an [FeFe] hydrogenase active-site model complex revealed by XAES-DFT. *Dalton Trans* 42(21):7539-7554.
25. Leidel N, *et al.* (2012) Electronic structure of an [FeFe] hydrogenase model complex in solution revealed by X-ray absorption spectroscopy using narrow-band emission detection. *J Am Chem Soc* 134(34):14142-14157.
26. Leidel N, *et al.* (2012) Site-selective X-ray spectroscopy on an asymmetric model complex of the [FeFe] hydrogenase active site. *Inorg Chem* 51(8):4546-4559.
27. Bergmann U & Glatzel P (2009) X-ray emission spectroscopy. *Photosynth Res* 102(2-3):255-266.
28. Pin S, Alpert B, Congiucastellano A, Longa SD, & Bianconi A (1994) X-Ray-absorption spectroscopy of hemoglobin. *Hemoglobins, Pt C* 232:266-292.
29. Lima FA, *et al.* (2014) Probing the electronic and geometric structure of ferric and ferrous myoglobins in physiological solutions by Fe K-edge absorption spectroscopy. *Phys Chem Chem Phys* 16(4):1617-1631.

30. Eisenberger P, Shulman RG, Brown GS, & Ogawa S (1976) Structure-function relations in hemoglobin as determined by X-ray absorption spectroscopy. *Proc Natl Acad Sci U S A* 73(2):491-495.
31. Bianconi A, *et al.* (1986) Local Fe site structure in the tense-to-relaxed transition in Carp deoxyhemoglobin - a XANES (X-ray absorption near edge structure) study. *Proc Natl Acad Sci U S A* 83(20):7736-7740.
32. Durham P, *et al.* (1983) X-ray absorption near edge structure (XANES) for Co, Cn and deoxyhemoglobin - geometrical information. *EMBO J* 2(9):1441-1443.
33. Zhang K, Reddy KS, Bunker G, & Chance B (1991) Active site conformation in myoglobin as determined by X-ray absorption spectroscopy. *Proteins: Structure, Function, and Genetics* 10(4):279-586.
34. Koster AS (1972) Electronic state of iron in hemoglobin, myoglobin and derivatives, as inferred from X-ray-fluorescence spectra. *J Chem Phys* 56(6):3161-&.
35. Jensen KP, Roos BO, & Ryde U (2005) O-2-binding to heme: electronic structure and spectrum of oxyheme, studied by multiconfigurational methods. *J Inorg Biochem* 99(1):45-54.
36. Jensen KP, Roos BO, & Ryde U (2005) O-2-binding to heme: electronic structure and spectrum of oxyheme, studied by multiconfigurational methods. *J Inorg Biochem* 99(4):978-978.
37. Chen H, Ikeda-Saito M, & Shaik S (2008) Nature of the Fe-O₂ bonding in oxy-myoglobin: effect of the protein. *J Am Chem Soc* 130(44):14778-14790.
38. Shaik S & Chen H (2011) Lessons on O-2 and NO bonding to heme from ab initio multireference/multiconfiguration and DFT calculations. *J Biol Inorg Chem* 16(6):841-855.
39. Wilson SA, *et al.* (2013) X-ray absorption spectroscopic investigation of the electronic structure differences in solution and crystalline oxyhemoglobin. *Proc Natl Acad Sci U S A* 110(41):16333-16338.